



Intracranial Dispersion Model

A model of ultrasonic dispersion for diagnosis of intracranial injury

Craig Burrell

Parmeshar Chauhan

Defence R&D Canada
Technical Memorandum
DRDC Toronto TM 2011-042
January 2012

Canada

Intracranial Dispersion Model

A model of ultrasonic dispersion for diagnosis of intracranial injury

Craig Burrell

Parmeshar Chauhan

Defence R&D Canada – Toronto

Technical Memorandum

DRDC Toronto TM 2011-042

January 2012

Principal Author

Original signed by Dr. Craig Burrell

Dr. Craig Burrell
Defence Scientist, Individual Behaviour and Performance Section

Approved by

Original signed by Mr. Stephen Boyne

Mr. Stephen Boyne
Head/Individual Behaviour and Performance Section

Approved for release by

Original signed by Dr. Stergios Stergiopoulos

Dr. Stergios Stergiopoulos
Acting Chair, Knowledge and Information Management Committee
Acting Chief Scientist

© Her Majesty the Queen in Right of Canada as represented by the Minister of National Defence, 2012

© Sa Majesté la Reine (en droit du Canada), telle que représentée par le ministre de la Défense nationale, 2012

Table of contents

Table of contents	i
Acknowledgements	iii
Abstract	iv
Résumé	iv
Executive summary	vii
Sommaire	ix
1 Introduction	1
2 Intracranial Dispersion Model	2
2.1 Model description	2
2.1.1 Linear dispersion	3
2.1.2 Dispersion in human tissues	5
2.1.3 Model limitations	7
2.2 Dispersion and attenuation	8
2.2.1 Dispersion and attenuation in blood	11
2.3 Negative dispersion	11
2.4 Analysis of dispersion spectra	13
2.4.1 Re-scaled propagation times	13
2.4.2 Spectral time shifts	16
2.4.3 Dispersion spectrum variation	21
3 Discussion	23
3.1 Time resolution and uncertainty	24
3.2 Case study	27
3.2.1 Case study conclusions	32

3.3	Implications for machine-learning systems	33
4	Conclusions	35
	References	37
	Acronyms	40

Acknowledgements

We wish to thank Dr. Stergios Stergiopoulos of Defence Research and Development Canada (DRDC) Toronto for initiating the research program in dispersive ultrasound, and for his ongoing support of this work. We also acknowledge the valuable contributions of Andreas Freibert and Jason Zhang of Advanced Ultrasound Technologies who designed and built the Dispersive Ultrasound System prototype.

Abstract

We present a model of ultrasonic dispersion in intracranial tissues that is intended to provide insight into the operation of DRDC Toronto's Dispersive Ultrasound System and contribute to the success of DRDC's ongoing research program in diagnostic applications of dispersive ultrasound. The Dispersive Ultrasound System is designed to use the dispersion spectrum produced by acoustic signals as they traverse the skull and intracranial tissue to identify non-visible neurological injuries, such as those resulting from blast exposure.

The Intracranial Dispersion Model is a mathematical representation of intracranial tissues and their acoustic dispersive properties. It has been developed in order to better understand the formation of dispersion spectra and the effects that various factors, including intracranial injury, have upon them. The formulation of the Intracranial Dispersion Model is presented in detail. We study, both analytically and numerically, how dispersion spectra respond to specific changes in the properties of tissues along the ultrasound propagation path. We also examine uncertainties in dispersion measurements and their diagnostic implications. Finally, a hypothetical case study illustrates the diagnostic insights that can be gained from use of the Intracranial Dispersion Model.

Résumé

Nous présentons un modèle de dispersion ultrasonique des tissus intracrâniens conçu pour offrir une idée sur le fonctionnement du système ultrasonique à dispersion de RDDC Toronto et contribuer au succès du programme de recherche courant de RDDC visant les applications diagnostiques par dispersion ultrasonique. Le système ultrasonique à dispersion est conçu pour utiliser le spectre de dispersion produit par des signaux acoustiques au fur et à mesure que ceux-ci traversent les tissus intracrâniens afin d'identifier les blessures neurologiques invisibles comme celles causées par l'exposition à une explosion.

Le modèle de dispersion intracrânien est une représentation mathématique des tissus intracrâniens et de leurs propriétés dispersives acoustiques. Le modèle a été élaboré pour mieux comprendre la formation du spectre de dispersion et les effets que divers facteurs, dont la blessure intracrânienne, ont sur celle-ci. La formulation du modèle est présentée en détail. Nous étudions, de façon analytique et numérique, comment le spectre de dispersion répond à certaines modifications spécifiques des caractéristiques des tissus le long du trajet de propagation des ultrasons. Nous étudions aussi l'incertitude des mesures de dispersion et leur portée diagnostique. Enfin, nous présentons une étude de cas hypothétique pour illustrer les aperçus de diagnostic qu'on peut

obtenir en utilisant le modèle de dispersion intracrânien.

This page intentionally left blank.

Executive summary

Intracranial Dispersion Model

Craig Burrell, Parmeshar Chauhan; DRDC Toronto TM 2011-042; Defence R&D Canada – Toronto; January 2012.

Background: Within the Canadian Forces there is a requirement to diagnose non-visible neurological injuries, such as those resulting from exposure to blast pressure waves. In response, DRDC Toronto is in the process of developing a Dispersive Ultrasound System. The Dispersive Ultrasound System is intended to provide a non-invasive, portable, simple to use, and relatively inexpensive means to diagnose non-visible neurological injuries.

To identify injuries, the Dispersive Ultrasound System relies on the dispersion of acoustic signals as they traverse the skull and intracranial tissue. All of the tissues along the ultrasonic propagation path contribute to the final observed dispersion spectrum. An Intracranial Dispersion Model has been developed in order to better understand the formation of dispersion spectra and the effects that various factors, including intracranial injury, have upon them. The Intracranial Dispersion Model is a mathematical representation of intracranial tissues and their acoustic dispersive properties.

Principal results: The Intracranial Dispersion Model was used to study the ways in which dispersion spectra are affected by a variety of factors. We studied the effect of changes in tissue characteristics, composition, and size on the position of individual spectral lines within a dispersion spectrum. We found that the dispersion arising from intracranial tissues is caused principally by the dispersive effects of brain tissue and diploë (a spongy bone tissue in the skull). As well, we found that some ultrasonic frequency sets are better able to detect injuries than others. The model was also used to study the time resolution requirements of the Dispersive Ultrasound System. We examined the consequences of poor time resolution, and found that low time resolution can result in certain pathologies going undetected. Lastly, a case study was used to demonstrate the way in which insights gained from the Intracranial Dispersion Model can contribute to the understanding of an observed dispersion spectrum.

Significance of results: The Intracranial Dispersion Model provides a better understanding of ultrasonic dispersion in intracranial tissues, and therefore contributes toward the use of ultrasound as a diagnostic probe for neurological injuries. The Model promotes a greater understanding of the response of observed dispersion spectra to various changes to the state of the intracranial tissues, which assists in the interpretation of the diagnostic significance of dispersion spectra. It can be used

to model the effects on dispersion spectra of certain pathologies and of anatomical changes. The Model also allows one to study the diagnostic limitations resulting from the finite time resolution of the Dispersive Ultrasound System. Finally, the Model provides insight into the challenges faced by the Dispersive Ultrasound System's machine-learning diagnostic decision support module.

Future work: The Intracranial Dispersion Model described in this document is a step toward a theoretical approach to the use of ultrasonic dispersion for the diagnosis of intracranial injury. There are various ways in which the Model can be extended and improved: inclusion of more tissues, modeling of other pathologies such as mild Traumatic Brain Injury, and generalization to non-linear dispersion, for instance. The output of the Model can be improved whenever new data on dispersion in intracranial tissues becomes available. We also anticipate that greater experience with DRDC's Dispersive Ultrasound System under laboratory and clinical conditions will lead to a fruitful dialogue with the Intracranial Dispersion Model, to the mutual benefit of both approaches.

Sommaire

Intracranial Dispersion Model

Craig Burrell, Parmeshar Chauhan ; DRDC Toronto TM 2011-042 ; R & D pour la défense Canada – Toronto ; janvier 2012.

Contexte : Les Forces canadiennes doivent diagnostiquer les blessures neurologiques invisibles comme celles causées par l'exposition aux ondes de pression du souffle. Par conséquent, RDDC Toronto participe à l'heure actuelle à la conception du système ultrasonique à dispersion. Le système servira à offrir un moyen non invasif, portable, simple à utiliser et relativement peu coûteux pour diagnostiquer les blessures neurologiques invisibles.

Pour identifier les blessures, le système ultrasonique à dispersion se fie sur la dispersion des signaux acoustiques qui traversent le crâne et les tissus intracrâniens. Tous les tissus le long du trajet de propagation des ultrasons contribuent à créer le dernier spectre de dispersion observé. Un modèle de dispersion intracrânienne a été élaboré afin de mieux comprendre la formation du spectre de dispersion et les effets que divers facteurs, y compris la blessure intracrânienne, ont sur celle-ci. Le modèle de dispersion intracrânienne est une représentation mathématique des tissus intracrâniens et de leurs propriétés de dispersion acoustique.

Résultats principaux : Le modèle de dispersion intracrânienne a été utilisé pour étudier l'incidence quant divers facteurs sur le spectre de dispersion. Nous étudions les impacts des modifications apportées aux caractéristiques, à la composition et à la taille des tissus sur le placement des lignes spectrales individuelles d'un spectre de dispersion. Nous avons conclu que la dispersion provenant des tissus intracrâniens est causée principalement par les effets dispersifs du tissu cérébral et du diploë (tissu osseux spongieux situé dans le crâne). De même, nous avons découvert que certains jeux de fréquence ultrasonique sont meilleurs que d'autres pour détecter des blessures. Le modèle a également été utilisé pour étudier les exigences en matière de temps de réponse du système ultrasonique à dispersion. Nous avons examiné les conséquences d'un mauvais temps de réponse et avons découvert qu'il nuit à la détection de certaines maladies. Finalement, une étude de cas a été utilisée pour démontrer la manière dont les connaissances obtenues avec le modèle de dispersion intracrânienne peuvent contribuer à comprendre un spectre de dispersion observé.

Portée des résultats : Le modèle de dispersion intracrânienne offre une meilleure compréhension de la dispersion ultrasonique dans les tissus intracrâniens et favorise l'utilisation des ultrasons comme sonde de diagnostic pour les blessures neurologiques.

Le modèle préconise une meilleure compréhension des réactions des spectres de dispersion observés causées par des modifications de l'état des tissus intracrâniens. Il permet aussi d'interpréter la signification du diagnostic du spectre de dispersion. Le modèle peut être utilisé pour modéliser les impacts de certaines maladies et modifications anatomiques sur le spectre de dispersion. Il permet d'étudier les limites de diagnostic déterminées par le temps de réponse fini du système ultrasonique de dispersion. Enfin, le modèle offre un aperçu des défis auxquels fait face le module d'apprentissage auxiliaire de décisions diagnostiques du système ultrasonique de dispersion.

Recherches futures : Le modèle de dispersion intracrânienne décrit dans le présent document constitue une étape vers l'approche théorique pour l'utilisation de la dispersion ultrasonique dans le diagnostic des blessures intracrâniennes. Il existe diverses manières d'améliorer le modèle, notamment l'inclusion de plus de tissus, la modélisation d'autres maladies comme le traumatisme cérébral léger et la généralisation vers la dispersion non linéaire. Les résultats du modèle s'améliorent chaque fois que de nouvelles données sur la dispersion dans les tissus intracrâniens sont disponibles. Nous nous attendons également à ce que d'autres essais cliniques et en laboratoire avec le système ultrasonique de dispersion de RDDC mènent à un dialogue fructueux avec le modèle de dispersion intracrânienne et profitent aux deux approches.

1 Introduction

When waves propagate through a medium, different frequencies propagate at different speeds. This phenomenon is called dispersion. The propagation times for a set of frequencies are referred to collectively as the dispersion spectrum. The amount of dispersion, and, therefore, the form of the dispersion spectrum, depends upon the physical properties of the medium. As such, dispersion can be used as a probe of those properties.

In a medical context, ultrasonic waves traveling through biological tissue exhibit dispersion, and, consequently, the resulting dispersion pattern contains information about the properties of the tissue. For this reason, ultrasonic dispersion has the potential for use as a medical diagnostic tool. Unlike most medical diagnostics based on ultrasound, dispersive ultrasound does not attempt to image the tissues. Rather, the tissue characterization is based simply on the observed dispersion spectrum.

DRDC Toronto has initiated a research program to develop a Dispersive Ultrasound System (DUS) for use in medical diagnosis [1, 2]. Ultrasound has significant advantages for military medicine: it requires relatively low power, it can be made portable, and it is inexpensive compared to many other diagnostic modalities. The DUS, pictured in **Figure 1**, is a small, portable device consisting of a pair of ultrasonic transducers (for transmission and reception of the signal), a signal processing unit, and a user interface.

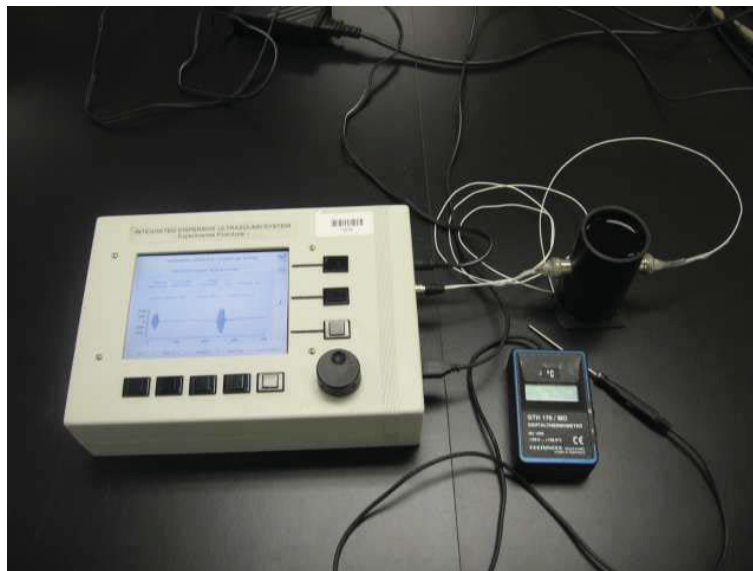


Figure 1: The Dispersive Ultrasound System (DUS) prototype. The data acquisition and analysis unit is pictured on the left; on the right is a fluid container with attached ultrasound probes, and a temperature monitor.

Preliminary experiments with the DUS prototype focused on evaluating its capacity to identify homogeneous fluids, such as water, apple juice, orange juice, etc., simply on the basis of the fluid's dispersion pattern [2]. These experiments were quite successful, and convinced us that the technology warranted further study. The next stage of development of the DUS is to apply it in a medical diagnostic context. To this end, plans are underway to initiate animal tests as a prelude to clinical studies on human subjects.

The principal medical use envisaged for the DUS is as a diagnostic tool for internal, non-visible injuries of the head, such as mild Traumatic Brain Injury (mTBI) or intracranial hemorrhage. The changes to the intracranial tissues that occur as a result of these injuries are likely to produce changes in the observed dispersion spectrum, and this is the key to the diagnostic capabilities of the DUS.

A central challenge, however, is to correctly interpret the observed dispersion spectra. Since normal tissue is dispersive, how reliably can the cause of a given dispersion spectrum be attributed to intracranial injury? Changes to a dispersion spectrum might indicate the development of an injury, but they might also be due to temperature changes or inconsistent placement of ultrasonic probes. The fielded DUS will rely on a machine-learning system to judge whether a given spectrum indicates healthy tissue or not. Nonetheless, it is worthwhile to study dispersion in intracranial tissues, for by means of such study we might gain insight into the problem space, understanding of possible performance limits on machine-learning approaches, and a better grasp of the possible causes of observed variations of dispersion spectra.

To this end, we developed in this report a simple model of ultrasonic dispersion in intracranial tissues. The model is not intended to predict observed dispersion spectra – since dispersion data are not available for all relevant tissues, such prediction is impossible – but rather to provide a flexible means for studying the variability that may arise in dispersion spectra as a result of a variety of factors. The model can be improved with time, and it is hoped that it will contribute to the effectiveness of the DUS research program.

2 Intracranial Dispersion Model

2.1 Model description

The Intracranial Dispersion Model (IDM) is motivated by the principal clinical application envisaged for the DUS, namely, the detection of non-visible intracranial injury, such as results from a blast exposure. In this clinical scenario, two ultrasonic probes, one for transmission and one for reception, are placed bilaterally on the temples of the patient and the acoustic pulses traverse the tissues between them. As such, the

acoustic propagation path consists of a series of tissue layers. **Figure 2** shows an anatomical cross-section of the human head illustrating the principal tissues which are present, namely the skull and the brain. We are also interested in cases in which damage to the head has caused pathologies such as intracranial hematoma, so we model scenarios in which a layer of blood is also present along the propagation path, as shown.

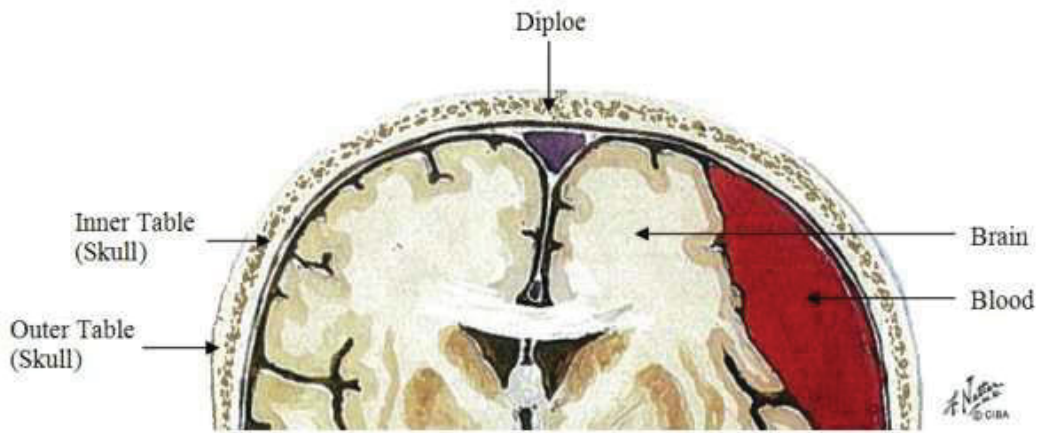


Figure 2: Cross-sectional view of human brain illustrating principal tissues along acoustic propagation path. Adapted from [3].

As shown in **Figure 3**, the skull is divided into three layers: outer ivory table, diploë, and inner ivory table. The inner and outer ivory tables are made of compact cortical bone and enclose the cancellous diploë [4]. Cancellous bones are heterogeneous and porous; the pores are typically filled with a fluid-like marrow [5]. The distinction of skull layers is important because of the very different dispersive characteristics of the cortical and cancellous bone types (see Section 2.1.2).

When the probes are mounted on the temples, the ultrasonic signal passes mainly through the frontal lobe of the brain, as shown in **Figure 4**. It is not known if acoustic propagation through the frontal lobe differs in any significant respects from propagation through other parts of the brain, but, since no specific data on the acoustic properties of the frontal lobe were available, we rely on data published for generic brain tissue.

2.1.1 Linear dispersion

The study of dispersion is equivalent to the study of the frequency dependence of the propagation time of an acoustic wave through a medium. Dispersion spectra show

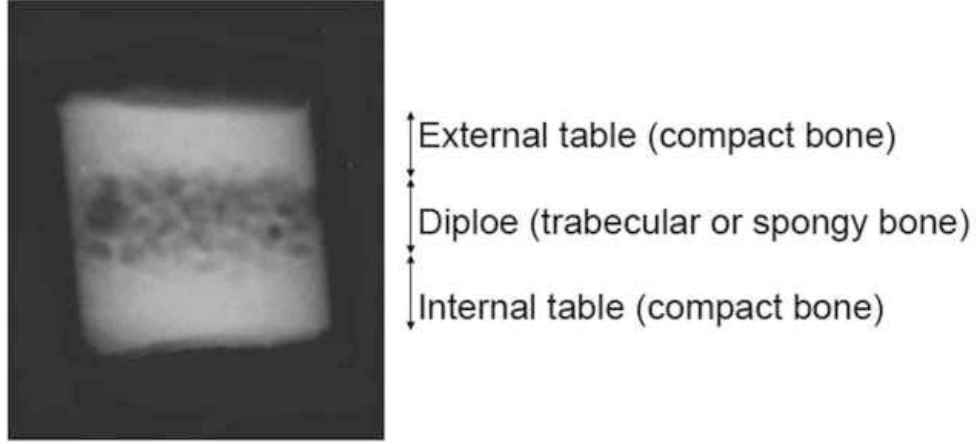


Figure 3: X-ray image of the three bone layers of the cranial vault [4].

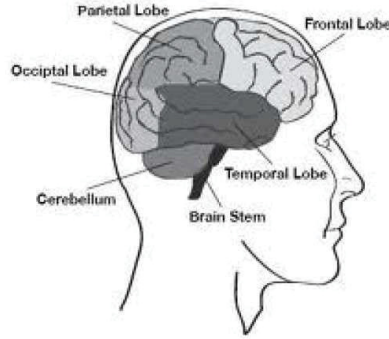


Figure 4: Basic brain anatomy, showing principal lobes [6].

the times required for different frequencies to traverse the medium of interest. In this Section, we present a simple model for computing propagation time.

For a given tissue i , the propagation time for frequency f , $t_i(f)$, can be calculated according to the relation

$$t_i(f) = \frac{d_i}{v_i(f)} \quad (1)$$

$$= \frac{d_i}{v_{0i} + (f - f_{0i})\Delta_i}, \quad (2)$$

where d_i is the depth of the tissue traversed by the acoustic wave, v_{0i} is the *base speed* defined at a *base frequency* f_{0i} , and Δ_i is the tissue's *dispersion trend*, which characterizes the frequency dependence of the propagation speed. In (2) we have a *linear dispersion model* because the propagation speed is assumed to change linearly across the range of frequencies under consideration. The frequency set currently used

in DUS laboratory experiments is shown in **Table 1**. Transmission frequencies are configurable, but are limited by transducer characteristics and tissue absorption to be less than 5 MHz.

Members of \mathcal{F}	Frequency (MHz)
f_1	1.93
f_2	2.13
f_3	2.78
f_4	3.33
f_5	3.85
f_6	4.08
f_7	4.17
f_8	4.39
f_9	4.76

Table 1: Frequency set \mathcal{F} used in modeling. Absorption of high frequency ultrasound by tissues and transducer characteristics limit the usable frequency range of the DUS to $f < 5$ MHz.

In Section **2.2**, we shall show that most materials, in fact, do not exhibit linear dispersion. We will also argue, however, and show by example, that dispersion is typically a small effect that can be described sufficiently accurately by a linear model over the limited frequency range that is of interest to us. As will be shown in Section **2.1.2** below, moreover, all of the available published dispersion data for relevant tissues assume that the dispersion is adequately described by a linear trend.

If we have a set of tissue layers \mathcal{T} , then the total propagation time is obtained by summing the propagation time for each tissue in the set

$$t(f) = \sum_{i \in \mathcal{T}} t_i(f). \quad (3)$$

The model can be conveniently upgraded or modified. For example, at the user’s discretion, the model can be supplemented with additional tissue layers. As well, if precise and detailed dispersion data are available, the dispersion for a given tissue can be modeled as a non-linear function of frequency, as in (1).

2.1.2 Dispersion in human tissues

The amount of dispersion arising in a tissue depends on the depth d_i of the tissue along the propagation path. Depth values used in the current model are shown in

Tissue	Mean (mm)	Modeling Range (mm)	Source
Brain	110	60 – 160	[3]
Skull, diploë	3.7 ($\sigma = 2.5$)	1.2 – 6.2	[4]
Skull, ivory tables	7	2 – 12	–
Blood, whole	–	0 – 25	–

Table 2: Depth of tissue layers along acoustic propagation path. Data for blood are for modeling of hemorrhage, and are not used when modeling a healthy brain.

Table 2. The mean values and ranges in **Table 2** are taken from the sources indicated in the last column. Brain tissue accounts for the bulk of the propagation path, with smaller contributions from the skull layers. The only tissue for which detailed depth information is available is the diploë skull tissue; studies indicate a mean depth of 3.7 mm and a standard deviation of 2.5 mm in the general population [4]. The depth and range of the ivory table bone was estimated from the fact that, as shown in **Figure 3**, the ivory table is roughly twice as deep as the diploë.

To model internal hemorrhage, we can introduce a layer of blood, as depicted in **Figure 2**. In practice, we varied the depth of the blood layer in the range indicated in **Table 2**. When a layer of blood was added, a layer of brain tissue of the same width was subtracted in order to maintain the same total depth. In reality, the brain tissue would be displaced and compressed by the hemorrhage, which would likely result in a change in the base propagation speed for the compressed tissues. Lacking any data, however, on how the compression of brain tissue affects its acoustic transmission properties, we were not able to correct for this effect.

To populate the IDM, an extensive literature review was carried out to find reported dispersion measurements for relevant biological tissues. These data are shown in **Table 3**. Only a few measurements are available, but they include the major tissues relevant to our application.

Brain tissue exhibits relatively small dispersion, but the predominance of brain tissue along the propagation path makes this an important contribution to the overall dispersion pattern.

The most dispersive tissue for which data exist is the diploë, which has a measured dispersion trend several orders of magnitude larger than the other tissues under consideration. Though it accounts for only a thin slice of the overall propagation path, it can nonetheless make a significant contribution to the dispersion pattern.

Diploë is a cancellous bone; other studies of cancellous bone have measured dispersion in femoral heads [5] or, more usually, in the calcaneus (heel bone) [7, 8, 9], and have

found dispersion trends smaller in magnitude and opposite in sign to that reported for diploë, as shown in **Table 3**. These negative dispersion observations were somewhat surprising, and their relevance to our model is not entirely clear; we discuss the issue further in Section **2.3**.

As shown, the ivory table layers of the skull have lower measured dispersion than the inner layer of diploë. Skull bone is a cortical bone, so we also include in **Table 3** data published for generic cortical bone. There is a substantial discrepancy between the cortical bone data and the ivory table skull data; probably the data specific to the ivory table are more reliable, but we include the cortical bone data in **Table 3** as a conservative upper limit on dispersion in this medium.

Tissue	Dispersion Trend ($\text{m} \cdot \text{s}^{-1} \cdot \text{MHz}^{-1}$)	Source
Brain	1.2	[10]
Skull, diploë	300	[11]
Skull, ivory tables	'slight' (assumed < 1)	[11]
Bone, cortical	10-30	[12]
Bone, calcaneus	-59 ± 52	[9]
Blood, whole	0.16	[13]; See Section 2.2.1 .

Table 3: Dispersion trend data for relevant tissues.

Calculation of the propagation time for a given tissue, as in (2), requires also that we know the propagation speed at a reference, or base, frequency. These values, taken from a literature review, are shown in **Table 4**. In each case, there was a range of speeds found in the published literature; for modeling purposes, we choose one value as a base, and vary the speed over the range indicated.

Tissue	Base Frequency (MHz)	Base Speed (m/s)	Range (m/s)	Sources
Brain	1.0	1562	1510 – 1572	[10] (base); [13] (range)
Skull, diploë	0.5	2240	2190 – 2870	[14] (base); [11] (range)
Skull, ivory tables	1.7	2960	2060 – 3030	[14] (base); [11] (range)
Blood, whole	1.0	1550	1540 – 1600	[13]

Table 4: Propagation speeds of acoustic waves through various tissues. All base speeds are given for a temperature of 37°C .

2.1.3 Model limitations

Not all of the tissues present in the intracranial space are represented in the current model. We know, for instance, that the propagation path must also traverse skin

tissue and the various tissues in the subarachnoid space, such as the meningeal membranes and the Cerebrospinal Fluid (CSF), among others [15]. We have been unable, however, to discover any published data on acoustic dispersion in these media. Were such data found, these tissues could be easily incorporated into the model, but, in the meantime, we exclude them from further consideration. By implication, our model is not intended to *predict* the observed dispersion spectrum, but, rather, to serve as a tool for a better understanding of the relative impact of different tissues on dispersion spectra, the effects of population variability on spectra, and the effect of injury on the spectra.

The tissues which are not included in the current model constitute a small portion of the total propagation path. For instance, the volume of cerebrospinal fluid, V_{CSF} , in the intracranial space is roughly one-tenth the volume of the brain, V_{brain} [16]. If we assume that the cerebrospinal fluid is distributed uniformly in a shell (outer radius r_2 and inner radius r_1) around the brain (radius r_1), we find that

$$\begin{aligned} V_{CSF} &= \frac{1}{10} V_{brain} \\ \frac{4}{3}\pi (r_2^3 - r_1^3) &= \frac{1}{10} \left(\frac{4}{3}\pi r_1^3 \right) \\ \Rightarrow r_2 &= \sqrt[3]{\frac{11}{10}} r_1 \approx 1.03 r_1, \end{aligned} \tag{4}$$

so that, under these reasonable assumptions, the depth of the cerebrospinal fluid layer is only about 3% of the depth of the brain tissue. In general, we believe that our model includes tissues accounting for roughly 90% of the propagation path length.

Another limitation of the current model is that it does not model the effects of Traumatic Brain Injury (TBI). As the study of TBI is a central objective of the dispersive ultrasound research program, this is a significant limitation grounded in our lack of knowledge about the effects of TBI on the dispersive characteristics of the intracranial tissues. If such effects were known, there would be no obstacle to their incorporation into the model.

2.2 Dispersion and attenuation

There is an important relationship between dispersion and attenuation of acoustic waves propagating through a medium which permits dispersion to be calculated from attenuation in cases where direct dispersion measures are not available. This Section briefly outlines the relevant theory, and in Section 2.2.1 we apply it in the case of blood.

In general, the frequency response of a linear system with attenuation and dispersion

can be written as [17, 18]

$$\begin{aligned} H(\omega) &= R(\omega) + iX(\omega) \\ &= e^{-\alpha(\omega)x} e^{-i\beta(\omega)x}, \end{aligned} \quad (5)$$

where $R(\omega)$ and $X(\omega)$ are the real and imaginary parts of the frequency response, $\alpha(\omega)$ is the attenuation coefficient, and $\beta(\omega)$ is the dispersion coefficient related to the phase velocity $V_p(\omega)$ by $\beta(\omega) = \omega/V_p(\omega)$. The frequency response $H(\omega)$ is the Fourier transform of the system's impulse response $h(t)$. When $h(t)$ is causal, as it must be in realistic physical systems, then $R(\omega)$ and $X(\omega)$ are related to one another by Hilbert transforms [19]:

$$R(\omega_0) = \frac{1}{\pi} \int_{-\infty}^{\infty} \frac{X(\omega)}{\omega - \omega_0} d\omega \quad \text{and} \quad (6)$$

$$X(\omega_0) = \frac{1}{\pi} \int_{-\infty}^{\infty} \frac{R(\omega)}{\omega - \omega_0} d\omega. \quad (7)$$

These equations, which are sometimes also referred to as the Kramers-Kronig relations, allow one to establish relationships between attenuation and dispersion. In particular, the dispersion can be calculated if the attenuation is known at all frequencies. Empirically, a wide variety of materials, including soft tissues, exhibit a power law frequency dependence for the attenuation

$$\alpha(\omega) = \alpha_0 |\omega|^y, \quad (8)$$

where $0 < y \leq 2$ for most materials [13]. In practice, this relationship can only be established empirically over a finite range of frequency, and additional assumptions are needed in order to justify computing the dispersion from the limited attenuation data. Several models have been proposed for this purpose.

The first model is called the *nearly local model* [20]. It assumes that the system is linear and causal, and that the attenuation and phase velocity change slowly over the frequency range of interest. In such cases, the dispersion can be written as a function of attenuation:

$$\frac{1}{V_p(\omega_0)} - \frac{1}{V_p(\omega)} = \frac{2}{\pi} \int_{\omega_0}^{\omega} \frac{\alpha(\omega')}{\omega'^2} d\omega', \quad (9)$$

where ω_0 is a reference frequency at which the phase velocity is assumed to be known. When the frequency dependence of the attenuation is linear ($y = 1$ in (8)), we have

$$\frac{1}{V_p(\omega_0)} - \frac{1}{V_p(\omega)} = \frac{2\alpha_0}{\pi} \ln \frac{\omega}{\omega_0} \quad (y = 1) \quad (10)$$

and when the frequency dependence is non-linear ($y \neq 1$ in (8)), we have

$$\frac{1}{V_p(\omega_0)} - \frac{1}{V_p(\omega)} = \frac{2\alpha_0}{\pi(y-1)} (\omega^{y-1} - \omega_0^{y-1}) \quad (y \neq 1). \quad (11)$$

This model has been shown to provide good predictions for dispersion when the attenuation is a nearly linear function of frequency [17, 21]. For media, however, in which the attenuation is a non-linear function of frequency, the nearly local model fails to accurately predict the dispersion [17].

A second model is called the *time-causal model* [22, 23]. In this case, the wave equations describing attenuation and dispersion are derived by assuming that the attenuation has a power law form, as in (8), and that the condition $\alpha(\omega)/(\omega/c_0) \ll 1$ is satisfied, where c_0 is the propagation speed of the wave in the absence of attenuation and dispersion. This condition translates into a y -dependent limit on ω ; for $1 \leq y \leq 2$, it imposes an upper limit. The condition is well satisfied for the tissues and frequency range relevant to our application¹. The time-causal model is equivalent to the nearly local model when $y = 1$, but differs for other values of y [23]. In particular, when the attenuation is non-linear in frequency it predicts

$$\frac{1}{V_p(\omega_0)} - \frac{1}{V_p(\omega)} = -\alpha_0 \tan\left(\frac{y\pi}{2}\right) (\omega^{y-1} - \omega_0^{y-1}) \quad (1 < y \leq 2). \quad (12)$$

An interesting consequence of this equation is that the time-causal model predicts no dispersion when $y = 2$, a prediction that has experimental support [24]. More generally, the time-causal model has been found to be in good agreement with experiments for a variety of materials and different values of y [17].

A third model for relating attenuation to dispersion is the *minimum-phase model* [17, 25, 26]. This model assumes that the transfer function $H(\omega)$ is minimum-phase, an assumption that is difficult to justify *a priori*, but which seems to be justified by the quality of the model's predictions [23]. An advantage of the minimum-phase assumption is that it allows the attenuation and dispersion to be directly related by Hilbert transforms, such that the dispersion is simply the Hilbert transform of the attenuation. No closed form solution analogous to (11) and (12) is possible in this model, but we can write

$$\frac{1}{V_p(\omega_0)} - \frac{1}{V_p(\omega)} = \frac{\beta(\omega_0)}{\omega_0} - \frac{\beta(\omega)}{\omega} \quad (13)$$

where

$$\beta(\omega) = \frac{\alpha_0}{\omega_s} P \int_{-\omega_s/2}^{\omega_s/2} |\omega'|^y \cot \left[\frac{\pi}{\omega_s} (\omega' - \omega) \right] d\omega' \quad (1 \leq y \leq 2). \quad (14)$$

In this integral, the cutoff frequency ω_s is set by the sampling frequency. The predictions of the minimum-phase model are very similar to those of the time-causal model, except at low frequencies (below 1 MHz), and are in good agreement with data for a variety of different power law relationships [17].

¹For instance, in Section **2.2.1** below, we will find that for whole blood we have $\alpha_0 = 0.023/\text{cm}$ and $y = 1.26$. Taking $c_0 \sim 1550$ m/s and requiring that the small ratio not exceed 0.01 yields the constraint $\omega < 10^5$ MHz. Our frequency range is well within this limit.

2.2.1 Dispersion and attenuation in blood

We were unable to locate direct measurements of the dispersive effects of blood, but, since data on attenuation in blood were available, we made use of the theory outlined in Section 2.2 to convert the attenuation data into dispersion data. In what follows, we present results computed using the time-causal model; results obtained with the nearly local model were also computed and were almost identical.

Measurements (see [13], Figure 4.10) indicate that attenuation follows a power law that changes with frequency, such that the dependence is approximately

$$\alpha(f) = \begin{cases} (0.20 \text{ dB/cm})|f|^{1.26} & \text{when } 1 \text{ MHz} < f < 4 \text{ MHz} \\ (0.26 \text{ dB/cm})|f|^{1.04} & \text{when } 4 \text{ MHz} < f < 10 \text{ MHz}. \end{cases} \quad (15)$$

This can be re-expressed in terms of angular frequency $\omega = 2\pi f$ as

$$\alpha(\omega) = \begin{cases} \frac{(0.023 \text{ /cm})}{(2\pi \cdot 10^6)^{1.26}} |\omega|^{1.26} & \text{when } 1 < \omega < 4 \\ \frac{(0.030 \text{ /cm})}{(2\pi \cdot 10^6)^{1.04}} |\omega|^{1.04} & \text{when } 4 < \omega < 10, \end{cases} \quad (16)$$

where ω is now expressed in units of $10^6 \cdot \text{rad/s}$, as shown, and we have removed the dB from the coefficient using $\alpha[\text{dB/cm}] = \alpha[\text{/cm}]/(20 \log_{10} e)$. Comparing (16) and (8), the dispersion in each frequency range can be computed using the time-causal model (12). In the low frequency range, we take $\omega_0 = 1$, $V_p(\omega_0) = 1550 \text{ m/s}$ (see [13], Figure 5.3), and, in accordance with (16), $y = 1.26$. Likewise, in the high frequency range, we take $\omega_0 = 4$, $V_p(\omega_0) = 1550.9 \text{ m/s}$, and $y = 1.04$; this base speed $V_p(\omega_0)$ was chosen so that the low frequency and high frequency curves meet at the boundary $\omega = 4$.

The resulting dispersion is shown in **Figure 5**. The trend of the solid curve is reliable toward the low end of the frequency spectrum, and the dashed curve toward the high end. Note that the overall dispersion is small, amounting to an increase in propagation speed of less than 0.2% over the frequency range under consideration.

In order to study the effect of blood on dispersion spectra using the linear dispersion model described in Section 2.1.1, the dispersion curves can be approximated by a linear dispersion trend, as shown in **Figure 5**. This linear best-fit differs from the computed curves by less than 0.03%, and so is a good approximation. The slope of this dispersion trend is about $0.16 \text{ m}/(\text{s} \cdot \text{MHz})$. This is the origin of the dispersion trend value for blood found in **Table 3**.

2.3 Negative dispersion

All of the models discussed in Section 2.2 predict that if attenuation increases with frequency ($\alpha(\omega) > 0$), then dispersion should be positive: the propagation speed should increase with frequency.

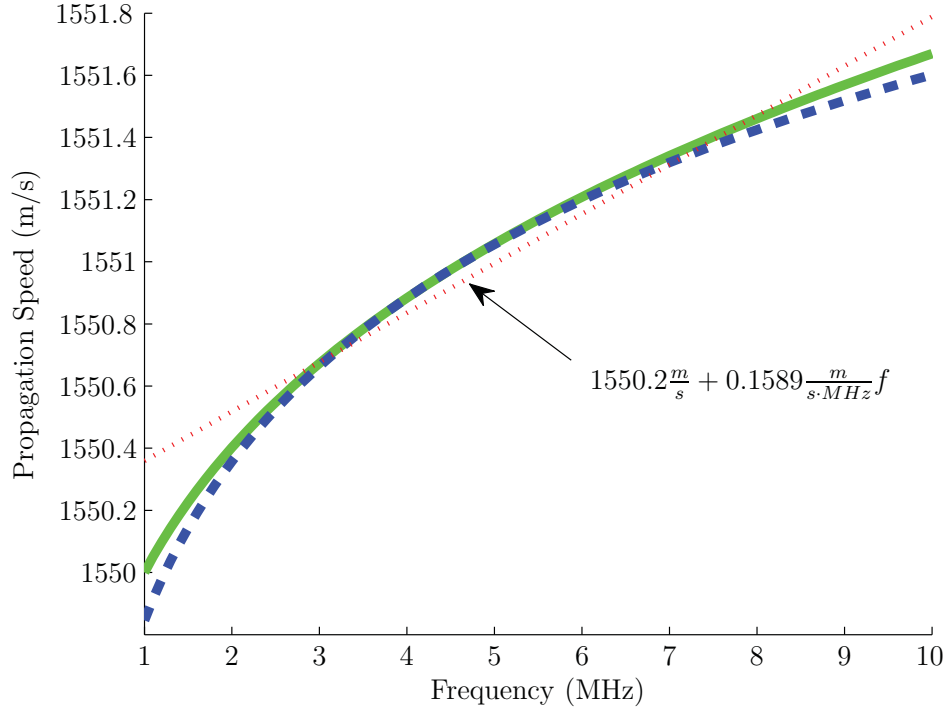


Figure 5: Acoustic dispersion in whole blood, computed from attenuation data [13]. The solid curve is computed for low frequencies (below 4 MHz) and the dashed curve for high frequencies. The dotted line is a linear best-fit over the frequency range under consideration.

Several authors have reported, however, observations of negative dispersion in cancellous bone – with the propagation speed decreasing as the frequency increases – even when the attenuation factor $\alpha(\omega)$ is unambiguously positive [7, 8, 9, 27]. These observations, which seem to be inconsistent with the Kramers-Kronig relations (6) and (7), have engendered a number of possible explanations, but no consensus has yet been reached as to which explanation(s) should be preferred [28].

One possible explanation is that the approximations to the Kramers-Kronig relations (in which the dispersion is derived from a frequency-limited attenuation curve, as described in Section 2.2 above) are invalid for cancellous bone. However, the same approximations have successfully predicted dispersion in a wide variety of materials [17, 24], and there is no known reason why they should not apply also to cancellous bone. It has been shown that negative dispersion can arise when acoustic waves propagate through stratified layers of solids and liquids [29, 30], but this explanation, while suggestive, is unsatisfactory insofar as cancellous bone, though consisting of solids and liquids (in the forms of bone and marrow, respectively), is not a stratified medium. Another possible explanation arises from the fact that theoretical models

of ultrasonic wave propagation predict two distinct compressional waves, called (on account of their propagation speeds) the fast and slow modes; it has been shown that the interference of these two modes, both of which have positive dispersion, can result in an overall apparent negative dispersion [31, 32, 33].

This debate is relevant for the present study because diploë, which is present in the model, is a cancellous bone, and because the presence of a negative dispersion tissue allows for more complex dispersion spectra, which in turn has a significant impact on the conceptual predictive strength of the model. For instance, if all tissues have positive dispersion, then the spectral lines will be ordered according to frequency, but this ordering is not necessarily preserved if a negative dispersion tissue is present.

At the present time, there is, to our knowledge, only one published measurement for dispersion in diploë, which showed strong positive dispersion (as shown in **Table 3**), though without error bars. The fact that negative dispersion has been measured in other cancellous bones (typically in the calcaneus, or heel bone) using more modern equipment and techniques perhaps raises a doubt about the accuracy of the sole existing measurement for diploë. In the absence of a confirmatory measurement of dispersion in diploë, we proceed as follows: we use the published dispersion trend value in our numerical modeling, but we are careful, in our discussion, not to draw conclusions which depend on all tissues having positive dispersion.

2.4 Analysis of dispersion spectra

Using the material presented in the preceding sections, we are able to study the ways in which dispersion spectra are affected by various factors such as tissue composition and size, uncertainties in propagation characteristics, and pathologies. We reiterate that our objective is not to predict the dispersion spectra observed in practice – lacking data on some of the relevant tissues, such an objective is out of reach at present – but rather to gain a better understanding of how various factors affect dispersion spectra.

2.4.1 Re-scaled propagation times

A representative dispersion spectrum is shown in **Figure 6**. The solid lines show the spectrum computed using the reference values for tissue depth, dispersion trend, and propagation speed given in **Tables 2 to 4**. The frequencies transmitted through the tissues are given in **Table 1**; each horizontal line in **Figure 6** corresponds to one of these frequencies. In dispersive ultrasound experiments, measurements of propagation time are typically repeated many times, so that individual data points are extended into lines, as shown. Under laboratory conditions the horizontal lines

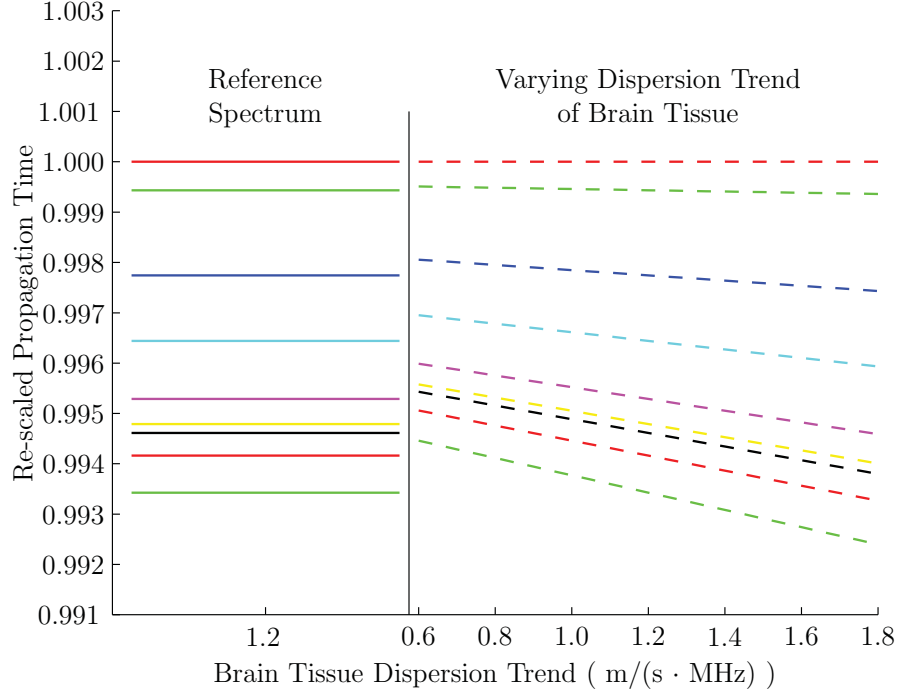


Figure 6: A sample dispersion spectrum is shown in solid lines. The vertical axis shows the re-scaled propagation time, and each horizontal line corresponds to a specific frequency. The spectrum was created using the central values shown in **Tables 2 to 4** and the frequency set from **Table 1**. The dashed lines show the effect on the spectrum of varying the dispersion trend for brain tissue.

are slightly broadened due to noise and time resolution limits; we discuss this further in Section **3.1**.

In **Figure 6**, and throughout this report, propagation times are re-scaled so that the slowest frequency has a re-scaled value of unity. In the simplest case in which there is only one tissue present, this makes the spectrum invariant under changes in tissue depth. For example, if \tilde{f} is the frequency which has the longest propagation time through tissue i , then the re-scaled time for frequency f is

$$\tilde{t}_i(f) = \frac{t_i(f)}{t_i(\tilde{f})} \quad (17)$$

$$= \frac{v_{0i} + (\tilde{f} - f_{0i})\Delta_i}{v_{0i} + (f - f_{0i})\Delta_i} \quad \text{from (2)} \quad (18)$$

$$= 1 - \frac{(f - \tilde{f})\Delta_i}{v_{0i}} + \mathcal{O}\left(\frac{\Delta_i^2}{v_{0i}^2}\right), \quad (19)$$

where we have dropped higher-order terms in the small ² ratio Δ_i/v_{0i} . From (18) we see that dependence on the tissue depth d_i has dropped out entirely, as expected. Dependence of the re-scaled time on base speed v_{0i} and dispersion trend Δ_i remains. Dependence on the base frequency f_{0i} is present but confined to higher-order terms, and is expected to be small. Note that since, by definition, $\tilde{t}_i(f) \leq 1$, we must have $(f - \tilde{f})\Delta_i \geq 0$. When, as is the case for all of the tissues listed in **Table 3**, we have $\Delta_i > 0$, this implies that we must have $f \geq \tilde{f}$. That is, the frequency with the longest propagation time must be the lowest frequency. Conversely, if we had $\Delta_i < 0$, then (19) implies that we would have the opposite frequency ordering: $\tilde{f} \geq f$.

In the more realistic case in which there are multiple tissue layers, it is no longer the case that re-scaling eliminates dependence on tissue depth, but it does *reduce* such dependence. If we let \tilde{f} once again represent the frequency with the longest overall propagation time, then the re-scaled time for frequency f in the general case of M tissue layers is

$$\tilde{t}(f) = \frac{\sum_{i=1}^M \frac{d_i}{v_{0i}} \left[\frac{1}{1 + (f - f_{0i}) \frac{\Delta_i}{v_{0i}}} \right]}{\sum_{j=1}^M \frac{d_j}{v_{0j}} \left[\frac{1}{1 + (\tilde{f} - f_{0j}) \frac{\Delta_j}{v_{0j}}} \right]} \quad (20)$$

$$= 1 - (f - \tilde{f}) \left\{ \sum_{i=1}^M \frac{\Delta_i d_i}{v_{0i} v_{0i}} \right\} / \left\{ \sum_{j=1}^M \frac{d_j}{v_{0j}} \right\} + \mathcal{O} \left(\frac{\Delta^2}{v_0^2} \right), \quad (21)$$

where, in moving to (21), we have once again dropped terms suppressed by additional powers of the factor $\Delta_i/v_{0i} \ll 1$. Clearly, the re-scaled time $\tilde{t}(f)$ does depend on the depths of the tissues, but the dependence is suppressed relative to that for the un-scaled time in (2). Note also that (21) has the form of a weighted sum ($\bar{x} = \sum x f(x) / \sum f(x)$); the position of a normalized spectral line is set by the weighted mean of the relative dispersion trend values (Δ_i/v_{0i}) where the weighting factor is the non-dispersive "base time" (d_i/v_{0i}) which the signal takes to pass through the medium in question.

Notice, from the exact expression (20), that if *all* of the tissue depths are scaled by an equal factor ($d_i \rightarrow \gamma d_i$), then $\tilde{t}(f)$ is invariant. Thus, it is only relative changes in tissue depth that affect the dispersion spectrum. This is an important feature of re-scaled propagation time because it means that the re-scaled dispersion spectrum is relatively insensitive to the normal variation in body size that one expects to encounter in a population of subjects.

Looking again at **Figure 6**, we note from the example dispersion spectrum (shown in solid lines) that the dispersion arising from the tissues included in the model is

²The data presented in **Table 3** confirm that $\Delta_i/v_{0i} \ll 1$ for the tissues under consideration.

a small effect: the propagation time of the slowest frequency differs from that of the fastest frequency by less than 1%. This is consistent with data collected in the laboratory. By implication, the spectrum is sensitive to even small changes that affect propagation time, and it is necessary to have precise methods for measuring the propagation time of each frequency.

As an illustration of how a dispersion spectrum can be affected by the properties of the dispersive tissues, consider the dashed lines in **Figure 6** which show the effect of varying the dispersion trend value for brain tissue, Δ_{brain} . The published value for this quantity is 1.2 m/(s·MHz) (see **Table 3**), but this value was published without error estimates. If we assume (arbitrarily) that the published value is accurate only to within $\pm 50\%$, we can see from **Figure 6** how this uncertainty translates into an uncertainty in the dispersion spectrum, effectively broadening each spectral line into a band that covers a range of propagation times.

There are several things to notice about this simple example. First, the variation is greater for frequencies that differ the most from the re-scaling reference frequency \tilde{f} ; this is reflected in the steeper slopes for the lines further removed from the top of the spectrum. This amplification is a consequence of the factor $(f - \tilde{f})$ in (19) and (21) which produces a relatively greater change in the spectral lines for relatively greater frequency differences.

Second, it is evident that for a given spectral line there are only two possible ways that it can vary in response to a change in the properties of the tissues: it can move up (to a larger re-scaled propagation time) or down (to a smaller one). To the extent that the shifting directions of multiple spectral lines are correlated – and they often are, as we argue in Section 2.4.2 – this implies that sets of spectral lines expand or contract together in response to changes in the medium.

2.4.2 Spectral time shifts

It is interesting to study the effect upon the spectral lines brought about by small changes in the properties of the tissues. Such changes cause the re-scaled time $\tilde{t}(f)$ for a given frequency to shift to a new value $\tilde{t}'(f)$. It is convenient to define the shift as

$$\delta\tilde{t}(f) = \tilde{t}'(f) - \tilde{t}(f). \quad (22)$$

We can calculate the approximate shift in the re-scaled time for the general case of M tissues from (20). We consider changes to the tissue's dispersive properties, base speed of propagation, and depth.

Dispersive properties. Consider small changes to the dispersion trend values for the tissues, $\Delta_i \rightarrow \Delta'_i = \Delta_i + \delta\Delta_i$ where $\delta\Delta_i \ll \Delta_i$. We treat both $\Delta_i/v_{0i} \sim \delta\Delta_i/\Delta_i \sim$

$\mathcal{O}(\kappa)$ as comparably small quantities and expand (20) in a Taylor series, retaining only the leading ($\mathcal{O}(\kappa^2)$) contribution to the time shift. It is

$$\delta\tilde{t}(f) = \frac{-(f - \tilde{f})}{\sum_{i=1}^M \frac{d_i}{v_{0i}}} \left\{ \sum_{i=1}^M \frac{d_i}{v_{0i}} \left[\frac{\delta\Delta_i}{\Delta_i} \right] \left[\frac{\Delta_i}{v_{0i}} \right] \right\}, \quad (23)$$

where the factors of $\mathcal{O}(\kappa)$ are enclosed in square brackets for clarity, and we have dropped terms suppressed by additional factors of $\mathcal{O}(\kappa)$.

In cases for which $f > \tilde{f}$ – that is, when the lowest frequency is also the slowest one, which is the normal situation when positive dispersion media predominate – a positive change in the dispersion trend, $\delta\Delta_i > 0$, contributes negatively to the spectral time shift, $\delta\tilde{t}(f) < 0$. This corresponds to a spectral expansion, since the new propagation time is further from unity than it was previously. This makes sense: a more positive dispersion trend results in more dispersion overall. Contrariwise, a negative change in dispersion trend, $\delta\Delta_i < 0$, causes a spectral contraction under the same conditions.

If, on the other hand, we have a rarer case in which $f < \tilde{f}$ – that is, when the highest frequency is the slowest one – we are dealing with a predominantly negative dispersion medium, and all of the effects described above are reversed: now it is a negative change in dispersion trend, $\delta\Delta_i < 0$, that causes a spectral expansion, and a positive change that causes a contraction. In each case, the expansion (contraction) results from whether or not the change tends to be toward (against) the dispersive behaviour characteristic of the medium as a whole.

Propagation speed. Consider small changes to the base propagation speed for the tissues, $v_{0i} \rightarrow v'_{0i} = v_{0i} + \delta v_{0i}$, where $\delta v_{0i} \ll v_{0i}$. Such a change can result from a temperature change in a medium, for example, or from pressurization. Again, we treat $\Delta_i/v_{0i} \sim \delta v_{0i}/v_{0i} \sim \mathcal{O}(\kappa)$ as small and expand (20) in a Taylor series. The leading contribution to the resulting time shift in the general case of M tissues is

$$\delta\tilde{t}(f) = \frac{(f - \tilde{f})}{\left[\sum_{k=1}^M \frac{d_k}{v_{0k}} \right]^2} \left\{ \sum_{i=1}^M \sum_{j=i}^M \left(\frac{1}{1 + \delta_{ij}} \right) \frac{d_i}{v_{0i}} \frac{d_j}{v_{0j}} S_{ij} \right\}, \quad (24)$$

where δ_{ij} is the Kronecker delta function

$$\delta_{ij} = \begin{cases} 1, & \text{if } i = j \\ 0, & \text{if } i \neq j \end{cases}, \quad (25)$$

and

$$S_{ij} = \left[\frac{\delta v_{0i}}{v_{0i}} \left(\frac{2\Delta_i}{v_{0i}} - \frac{\Delta_j}{v_{0j}} \right) + \frac{\delta v_{0j}}{v_{0j}} \left(\frac{2\Delta_j}{v_{0j}} - \frac{\Delta_i}{v_{0i}} \right) \right] \quad (26)$$

is a quantity of $\mathcal{O}(\kappa^2)$. Neglected terms are suppressed by additional factors of $\mathcal{O}(\kappa)$.

The spectral lines therefore shift up or down depending on the sign of the double summation in (24). The direction of the shift depends on the factor S_{ij} , which in turn depends on the relative values of the dispersion trend variables Δ_i , base propagation speeds v_{0i} , and speed changes δv_{0i} .

The fact that S_{ij} can be either positive or negative raises the interesting question of when (24) can sum to zero. In general it is always possible to choose the δv_{0i} so that the sum is zero, provided that $\delta v_{0i} \neq 0$ for at least two tissues. In the special case $M = 2$ we find that the sum is zero when

$$\frac{\left(\frac{\Delta_1}{v_{01}}\right)}{\left(\frac{\Delta_2}{v_{02}}\right)} = \frac{\left(\frac{\delta v_{01}}{v_{01}}\right) \left(\frac{d_1}{v_{01}} / \frac{d_2}{v_{02}}\right) - \left(\frac{\delta v_{02}}{v_{02}}\right) \left(1 + 2 \left(\frac{d_1}{v_{01}} / \frac{d_2}{v_{02}}\right)\right)}{\left(\frac{\delta v_{01}}{v_{01}}\right) \left(\frac{d_1}{v_{01}} / \frac{d_2}{v_{02}}\right) \left(2 + \left(\frac{d_1}{v_{01}} / \frac{d_2}{v_{02}}\right)\right) - \left(\frac{\delta v_{02}}{v_{02}}\right) \left(\frac{d_1}{v_{01}} / \frac{d_2}{v_{02}}\right)}. \quad (27)$$

Making the additional assumption that only the base speed in the first tissue changes ($\delta v_{02} = 0$), this simplifies to

$$\frac{\left(\frac{\Delta_1}{v_{01}}\right)}{\left(\frac{\Delta_2}{v_{02}}\right)} = \frac{1}{2 + \left(\frac{d_1}{v_{01}} / \frac{d_2}{v_{02}}\right)}. \quad (28)$$

Notice that in this case, when only one base speed varies, the zero-sum condition in (28) is independent of that variation, so that it can only be satisfied for media having very particular properties. **Figure 7** shows this $\delta\tilde{t}(f) = 0$ contour, derived from the approximation in (24), as well as the same contour derived from the exact expression in (22) (the analytic form of which is too complex to present here). It is clear that the approximation captures the general trend of the exact result.

An interesting feature of the approximation in (24) is that the only frequency dependence is in the $(f - \tilde{f})$ pre-factor. This implies that, for a given set of media, the sign of $\delta\tilde{t}(f)$ depends entirely on the relative values of f and \tilde{f} . If all of the media have positive (negative) dispersion, then \tilde{f} will be the lowest (highest) frequency and the sign of $(f - \tilde{f})$ will be the same for all values of f . Consequently, the time-shift $\delta\tilde{t}(f)$ will have the same sign for all frequencies. In such cases, (24) therefore predicts that, to a first approximation, all of the spectral lines respond in the same way, either expanding or contracting together.

This uniform time-shifting behaviour is, however, not always a feature of the exact time-shift in (22). To illustrate this, **Figure 8** shows the time-shift $\delta\tilde{t}(f)$ as a function of frequency for a two-tissue system satisfying the condition in (28). With this condition the approximate time-shift in (24) is exactly zero; however the exact time-shift

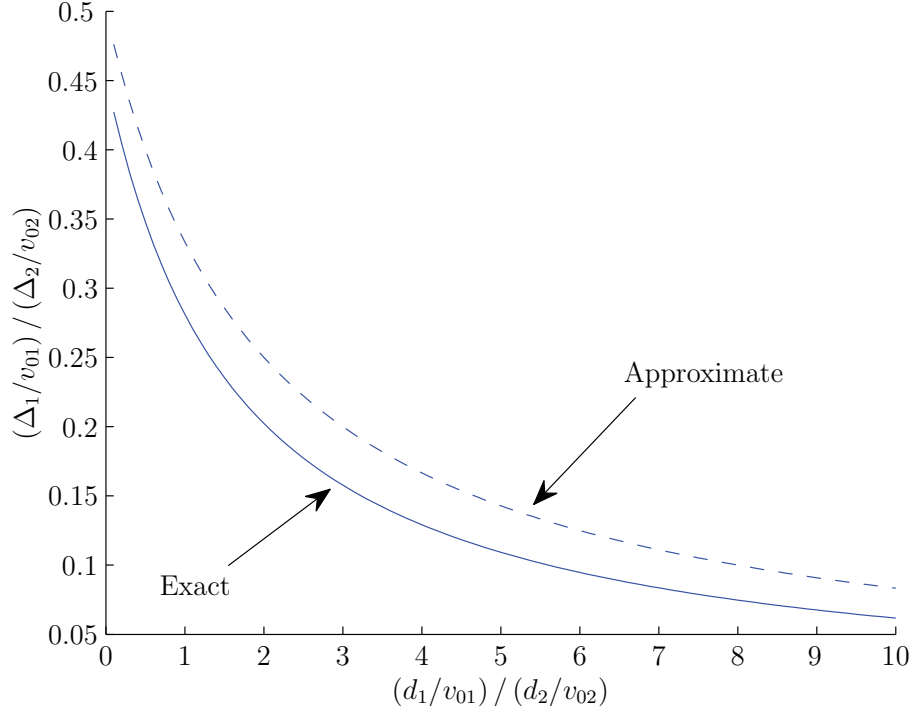


Figure 7: Dispersion spectrum $\delta\tilde{t}(f) = 0$ contours under base speed variation in a two-tissue system. The solid line is the exact contour and the dashed line is derived from the leading-order approximation. The particular contours shown are for $\delta v_{01}/v_{01} = 0.1$, $\delta v_{02} = 0$, and $f = f_3$ (see **Table 1**).

in (22), though small, has a residual frequency dependence, as shown in the Figure. At low frequencies, the time-shift is negative, indicating expansion of the spectrum, and at high frequencies, it is positive, indicating compression. Consequently, it is not possible to conclude that a spectrum *always* expands or contracts under base speed variation; there are special cases – in particular, when the variation is almost zero – when part of the spectrum may expand and another may contract.

For cases in which tissues having both positive and negative dispersion are present, the reference frequency \tilde{f} is, in general, no longer the highest or lowest frequency, but one of the intermediate frequencies. The direction of the spectral line shift still depends, as before, on the sign of $(f - \tilde{f})$, and so differs across the frequency set. In effect, an intermediate reference frequency \tilde{f} divides the frequency set into two parts: the low ($f < \tilde{f}$) and high ($f > \tilde{f}$) subsets. The spectral lines of the frequencies in each subset will expand or contract together, but the behaviour of the two subsets will be opposites.

Tissue depth. Consider small changes to the tissue depth, $d_i \rightarrow d'_i = d_i + \delta d_i$, where

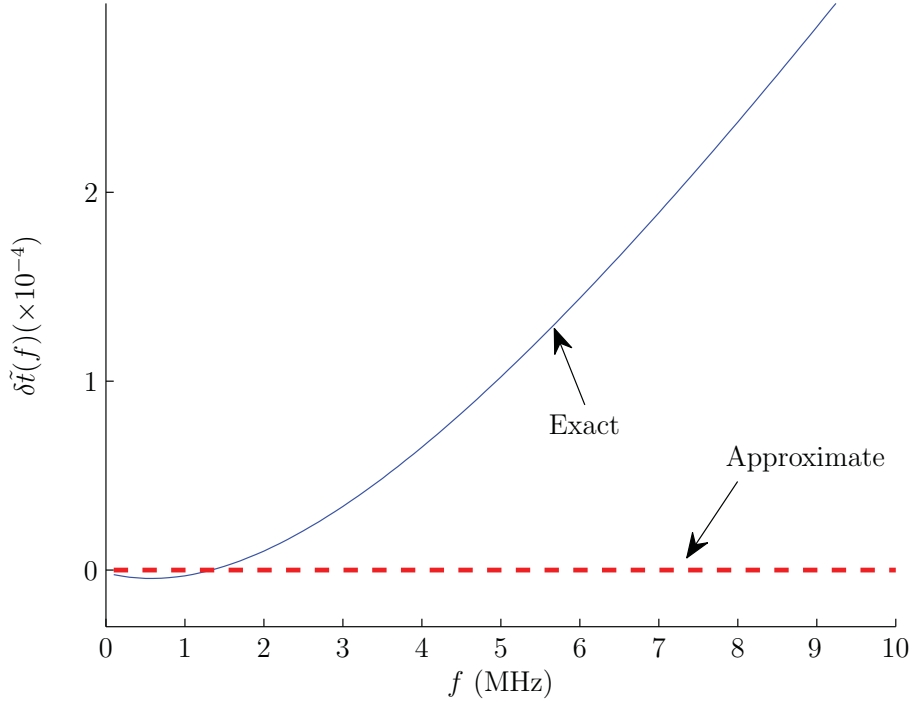


Figure 8: Frequency dependence of the dispersion spectrum time-shift $\delta\tilde{t}(f)$ under base speed variation in a two-tissue system satisfying the constraint in (28). The leading contribution to the time-shift vanishes, but the frequency dependence of subleading contributions causes the time-shift to be negative for some frequencies and positive for others.

$\delta d_i \ll d_i$. Again, we treat $\Delta_i/v_{0i} \sim \delta d_i/d_i \sim \mathcal{O}(\kappa)$ as small and expand (20) in a Taylor series. The leading contribution to the resulting time shift in the general case of M tissues is

$$\delta\tilde{t}(f) = \frac{-(f - \tilde{f})}{\left[\sum_{k=1}^M \frac{d_k}{v_{0k}} \right]^2} \left\{ \sum_{i=1}^{M-1} \sum_{j=i+1}^M \frac{d_i}{v_{0i}} \frac{d_j}{v_{0j}} \left(\frac{\Delta_i}{v_{0i}} - \frac{\Delta_j}{v_{0j}} \right) \left(\frac{\delta d_i}{d_i} - \frac{\delta d_j}{d_j} \right) \right\} \quad (M \geq 2), \quad (29)$$

where additional contributions are suppressed by a factor of $\mathcal{O}(\kappa)$. As indicated, this result is valid when $M \geq 2$. (When $M = 1$ the time shift under changes in tissue depth is exactly $\delta\tilde{t}(f) = 0$ because the propagation times for frequencies f and \tilde{f} change by the same factor, leaving the re-scaled propagation time in (20) unchanged.)

According to the approximation in (29) there are two special conditions under which

a term in the sum may be zero: when two tissues have the same relative dispersion trend ($\Delta_i/v_{0i} = \Delta_j/v_{0j}$), or when they experience the same relative change in depth ($\delta d_i/d_i = \delta d_j/d_j$).

The first of these conditions is an artifact of the approximation, and is therefore only approximately true. For example, in the simplest ($M = 2$) case, the exact expression for the time-shift in (22) yields zero if

$$(\Delta_1/v_{01}) = \frac{(\Delta_2/v_{02})}{1 - (f_{01} - f_{02})(\Delta_2/v_{02})} \quad (30)$$

$$= (\Delta_2/v_{02}) + \mathcal{O}(\Delta_2^2/v_{02}^2). \quad (31)$$

On the other hand, the proportionality in (29) of the time-shift to $(\delta d_i/d_i - \delta d_j/d_j)$ for two tissues i and j carries over to the exact result. Therefore, if the depths of all tissues change proportionately, then the overall time-shift will be zero, as was noted above in the discussion of (20).

An interesting case occurs when one tissue is displaced by another without affecting the overall sum of tissue depths, $\delta d_i = -\delta d_j$ for two (not necessarily neighbouring) tissues. In general, such cases result in a non-zero contribution to the time-shift, unless it also happens that the initial depths of the two tissues are equal ($d_i = d_j$).

As was the case for the base speed variations above, the expansion or contraction of the spectral lines in response to depth variations depends, to a first approximation, on the factor $(f - \tilde{f})$. Again, frequencies in the low subset ($f < \tilde{f}$) tend to expand or contract as a group, and those in the high subset ($f > \tilde{f}$) tend to behave as a group with the opposite tendency. We do find, however, as we also did in the case of propagation speed variation above, that it is possible to find special cases in which the time-shift is small enough that the weak frequency dependence from the higher-order corrections to (29) can result in $\delta \tilde{t}(f)$ being positive for some frequencies and negative for others, even within the same subset. Usually, however, all frequencies in a given subset (high or low) will shift in the same direction.

2.4.3 Dispersion spectrum variation

When studying shifts in the dispersion spectrum brought about by changes in tissues, it is useful to have a measure of the degree of spectral variation brought about by those changes. In this Section, we define such a measure.

A simple candidate measure would sum over the spectral shifts in each frequency, yielding

$$\tilde{s} = \sum_{f \in \mathcal{F}} |\delta \tilde{t}(f)|, \quad (32)$$

where \mathcal{F} is the set of frequencies used and $\delta\tilde{t}(f)$ is defined in (22).

This measure, however, has several undesirable characteristics. For instance, it scales with the number of frequencies, so that, all other things being equal, doing a measurement with more frequencies will yield a larger spectral variation. Second, it depends on the particular frequencies used. This can be seen from (23), (24), and (29), each of which show that the re-scaled time shift for a given frequency f is multiplied by the factor $(f - \tilde{f})$, where \tilde{f} is the frequency with the longest propagation time. Thus, the spectral variation computed using (32) will depend on the way the frequencies are distributed with respect to \tilde{f} . Both of these characteristics are undesirable because they make the spectral variation \tilde{s} sensitive to factors that pertain to the experimental method rather than to the tissues being studied.

A third potential issue with (32) is that it sums over the absolute values of the time shifts. This can be sensible in some situations, but by removing information about the sign of $\delta\tilde{t}(f)$ it removes information that may be of interest – namely, whether the re-scaled spectrum expands or contracts.

These considerations suggest another measure of variation of the dispersion spectrum:

$$s = \text{sgn}(\delta\tilde{t}(f)) \max_{f \in \mathcal{F}} |\delta\tilde{t}(f)|. \quad (33)$$

This definition selects the largest time-shift, regardless of whether it is positive or negative. It does not depend on the number of frequencies in the set \mathcal{F} , and though it clearly does depend on the value of the frequency with the largest time-shift, there is no dependence on any other frequencies in \mathcal{F} .

A notable feature of this definition of dispersion spectrum variation is that a positive value corresponds to a spectral contraction ($\delta\tilde{t}(f) > 0$ implies that the new time is larger – that is, closer to unity – than was the original time). Likewise, a negative dispersion spectrum variation indicates spectral expansion. The numerical value of the dispersion spectrum variation directly indicates the amount of shift of the most displaced spectral line, which is an intuitive indicator of the amount of variation in the spectrum as a whole.

Table 5 presents the dispersion spectrum variations produced by varying the depth, dispersion trend, and base speed values for each of the principal tissues in the model. To generate these values, we used the data in **Tables 2 to 4**; the reference values for depth, dispersion trend, and base speed were used to generate a reference dispersion spectrum, and then each quantity (depth, dispersion trend, base speed) was varied independently across its range as given in **Tables 2 to 4**.

The results in **Table 5** are shown as ordered pairs (x, y) ; the first element gives the dispersion spectrum variation that results when the varied quantity has the lowest

Tissue	Dispersion Spectrum Variation, s		
	Depth ($\times 10^{-3}$)	Base speed ($\times 10^{-4}$)	Dispersion Trend ($\times 10^{-4}$)
Skull, ivory table	(-0.15, 0.14)	(0.29, -0.19)	(0.0015, -0.0015)
Skull, diploë	(3.0, -3.0)	(-7.4, 5.9)	(4.9, -3.8)
Brain	(-3.3, 1.3)	(1.9, -2.3)	(4.1, -4.1)

Table 5: Dispersion spectrum variation produced by varying tissue depth, base speed, and dispersion trend in the ranges given in **Tables 2 to 4**. Central values of each parameter are as given in the same Tables.

value in its range, and the second element gives the variation that is produced when the varied quantity has the highest value in its range.

Consider first the column for variations in tissue depth. The ivory table skull bone and brain tissue both indicate a spectral contraction (a movement from negative variation to positive) as the depth is increased; these are both low dispersion media, so this result is expected. By contrast, increasing the depth of the high dispersion diploë tissue causes the overall spectrum to expand. The variations produced by base speed changes in the next column are related: increasing the base propagation speed through a medium is convertible with decreasing the tissue’s depth. We are not surprised, therefore, to see that the dispersion spectrum variation inclining in the opposite direction from the first column (which was produced by increasing tissue depth). Finally, the third column shows that increasing the dispersion trend value for a tissue, which just adds more dispersion along the propagation path, causes the spectrum to expand.

As a final comment on **Table 5** we note that the dispersion spectrum variation s produced by changes to the ivory table bone is at least an order of magnitude smaller than that produced by the other tissues. This reflects the fact that ivory table bone is both low in depth and low in dispersion, and does not have a substantial impact on the final spectrum.

3 Discussion

In this Section, we consider the experimental and diagnostic implications of the fact that that the DUS has finite time resolution. We then present a hypothetical case study to illustrate how the IDM can provide insight into observed dispersion spectra. Finally, we discuss the significance of our findings for machine learning systems such as that used by the DUS.

3.1 Time resolution and uncertainty

The precision of a propagation time measurement using the DUS is limited by the system's time resolution, and this results in an uncertainty in the position of a spectral line in a dispersion spectrum. In this Section, we examine the impact that these precision limits have on the diagnostic use of the DUS.

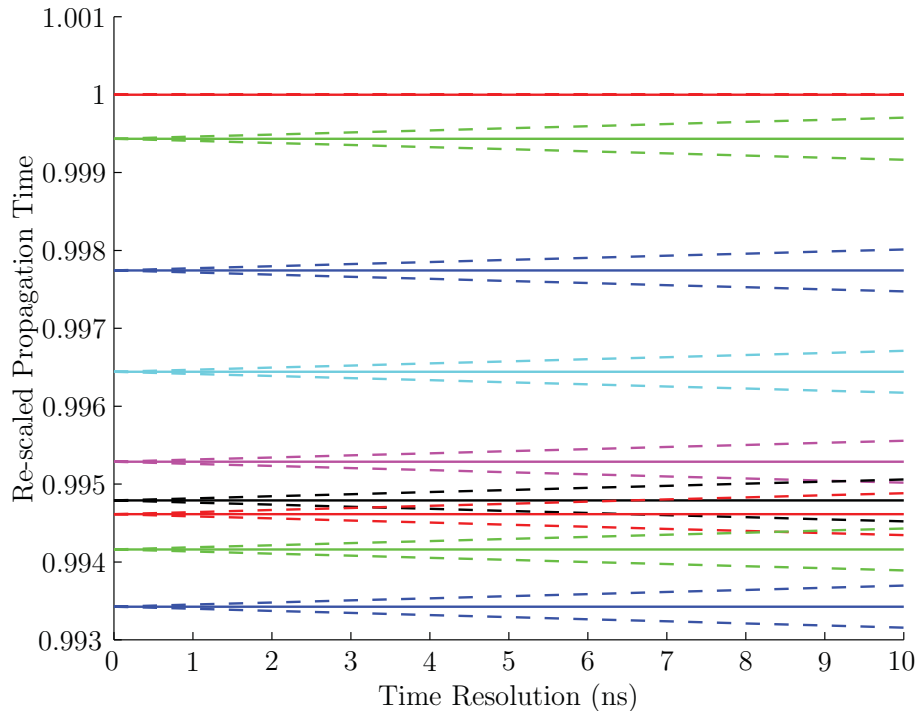


Figure 9: Time-resolution uncertainties in re-scaled propagation times for a set of frequencies passing through tissues. The frequencies are those shown in **Table 1**.

There are several potential sources of time resolution uncertainties in the DUS. The lowest level source, which establishes a minimal resolution limit that cannot be further improved, arises from a phase-marking procedure in the signal processing algorithms used by the DUS. To resolve the narrow splitting of spectral lines, the DUS requires time resolution that exceeds the sampling period of the signal. The phase-marking procedure uses phase information in the received signal to acquire *sub-sampling period* time resolution [2]. However, phase distortion arising from system noise and signal quality causes a low-level jitter in the computed signal propagation time. Empirically, the scale of this uncertainty depends upon the quality of the received ultrasound signal, but we have found it to be consistently less than 2 ns.

The IDM can be used to simulate the effect of time resolution on the positions of spectral lines. **Figure 9** shows how the uncertainty in the re-scaled propagation time

increases as the time resolution of the DUS worsens.

These results can be used to guide the selection of a set of suitable transmission frequencies. **Figure 9** shows that when frequencies are too close together uncertainties from time resolution can cause the spectral lines to blur together. Hence, the current set of transmission frequencies is not ideal. **Figure 10** shows the spectrum that results when the transmission frequencies are evenly spaced at a distance of 0.4 MHz, starting from a minimal frequency of 1.2 MHz. In this case, overlap due to the broadening of the spectral lines can be prevented for the time resolution limits shown³.

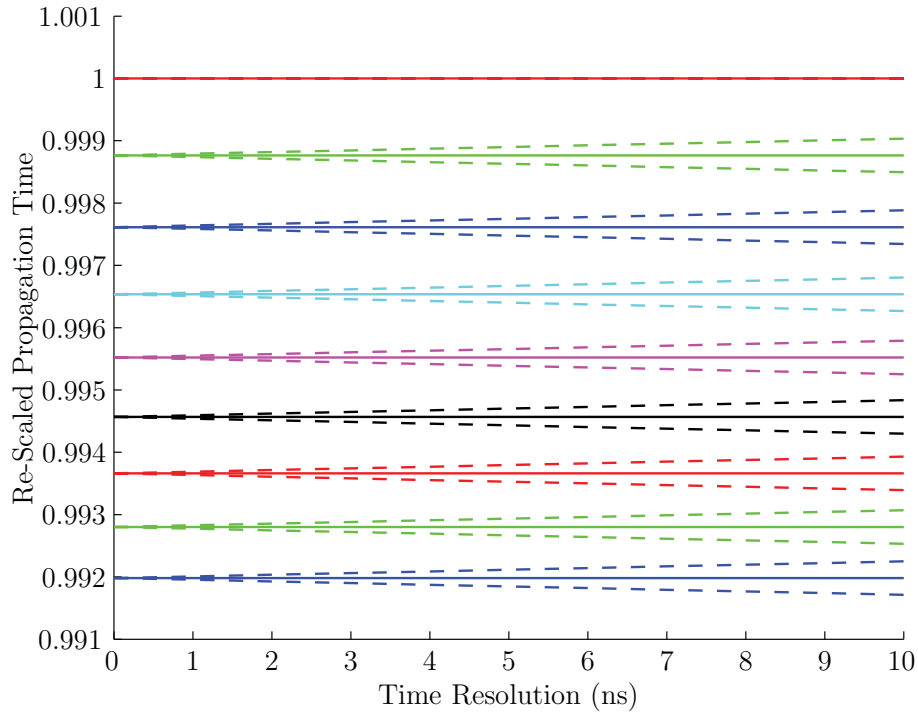


Figure 10: Time-resolution uncertainties in re-scaled propagation times for a set of frequencies passing through tissues. The frequencies are in the range 0 – 5 MHz, and are evenly spaced at intervals of 0.4 MHz.

The spectra in **Figures 9** and **10** were generated using the mean values for the tissues listed in **Tables 2** to **4**. A different set of tissue properties would result in a different dispersion spectrum, and, therefore, different requirements would have to be instituted to avert overlap of the time resolution-broadened spectral lines. The set of frequencies most suitable to a given situation should be determined on a case-by-case

³It should be noted that ultrasonic transducers have a frequency-dependent power transmission profile which makes certain transmission frequencies more suitable than others; this profile should also be consulted in the process of choosing the set of transmission frequencies.

basis, either by modeling or by experimental tests. Departures from linear dispersion will also affect the spacing of spectral lines; a logarithmic trend such as that shown in **Figure 5** will tend to increase the separation of low frequency spectral lines.

Uncertainty in the dispersion spectrum has implications for the ability of the DUS to detect pathologies. We illustrate this in **Figure 11**, which shows two dispersion spectra. The first, on the left, is the dispersion spectrum of a healthy subject. As in **Figure 9**, the dashed lines represent the uncertainty in the spectral lines position induced by the limited time resolution of the DUS. The second spectrum, on the right, results from an injury that causes bleeding in the intracranial space. As the amount of blood increases the spectrum contracts, but the injury can only be detected if the contraction exceeds the uncertainty bounds in the healthy subject's spectrum.

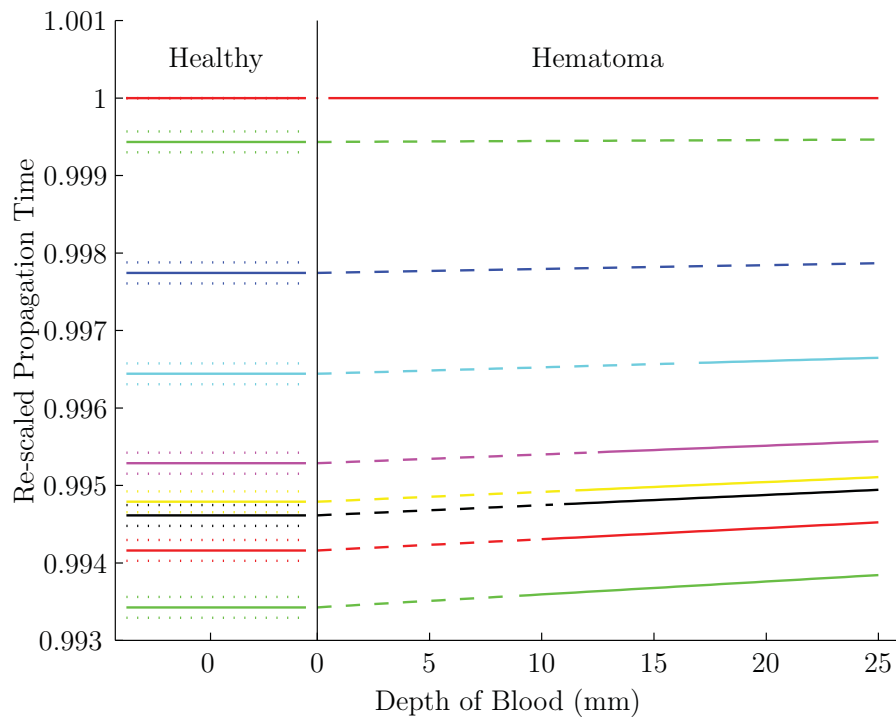


Figure 11: The dispersion spectrum of a healthy subject is shown on the left; dashed lines indicate the uncertainty around each spectral line corresponding to time resolution limits of 5 ns. On the right is the spectrum resulting from the gradual addition of blood, as from an intracranial hematoma. As the spectral lines exceed the resolution uncertainty bounds they change from dashed to solid lines.

In **Figure 11**, undetectable changes in a spectral line are represented by dashed lines; once the injury becomes detectable the spectral line is represented by a solid line. This illustrates that, given a frequency-independent time resolution, the frequencies

furthest from the reference frequency are best able to detect injury, and are therefore more useful to a machine learning system. This is consistent with our earlier observation that frequencies furthest from the reference frequency are the most sensitive to variations in the properties of the medium.

3.2 Case study

In this Section we present a hypothetical scenario involving dispersive ultrasound observations on a patient. We assume that a patient is subject to two examinations with the DUS; the two examinations are separated by some time interval. In each case, the dispersion spectra produced from these examinations will be dependent upon the examination conditions, including the positions of the transducers on the skull, the anatomy of the intracranial tissues, and the properties of those tissues (temperature and pathological state, for instance).

For the purposes of discussion, suppose a variation between the two dispersion spectra is observed, as in **Figure 12**. The second observation exhibits a spectral contraction relative to the first. We want to consider what can be concluded about the patient on the basis of the variation in the dispersion spectra, even without the use of a trained machine-learning system.

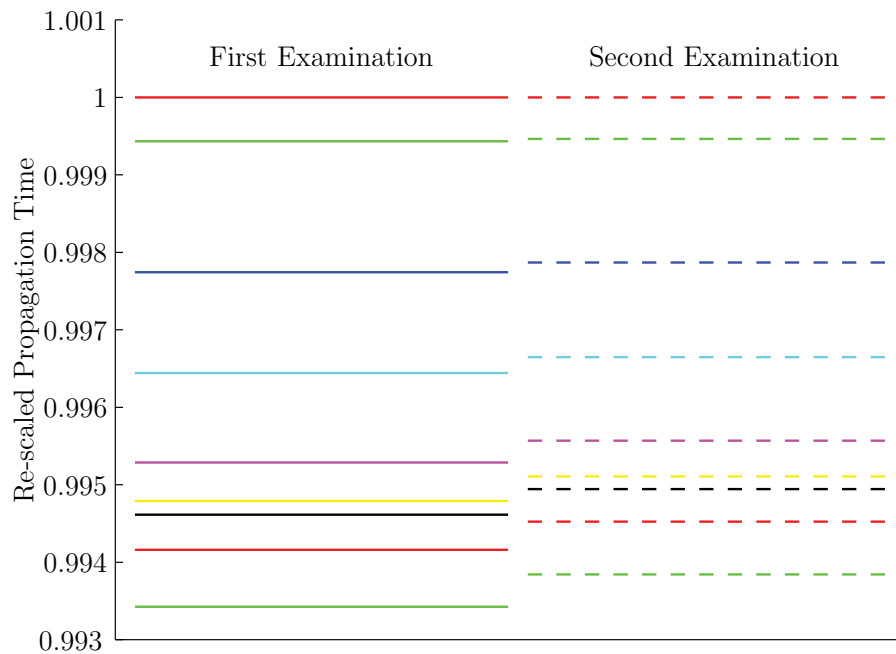


Figure 12: Hypothetical dispersion spectra collected from a single patient on two different occasions.

Each tissue along the signal’s propagation path contributes to the final observed

dispersion spectrum. The observed spectrum is not, however, a simple summation of the contributions from the individual tissues. Rather, because of the re-scaling of propagation times discussed in Section 2.4.1, the spectrum is a weighted average of the individual contributions, as in (21). This is illustrated in **Figure 13**, where continually increasing the depth of brain tissue along the propagation path causes the observed spectrum to asymptotically converge to the dispersion spectrum of brain tissue alone.

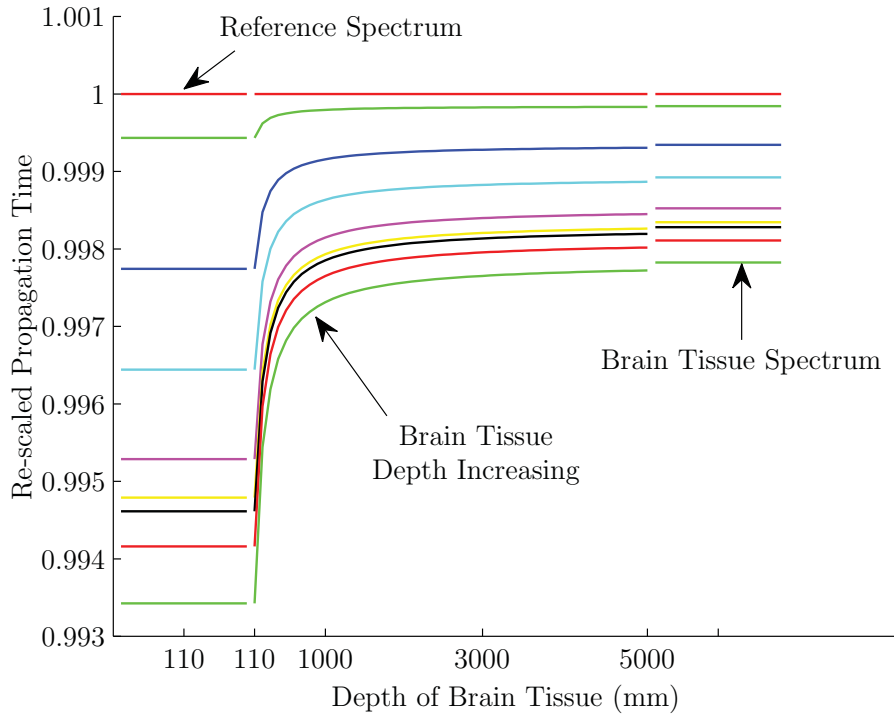


Figure 13: Re-scaled dispersion spectra are a weighted average of the individual contributions. The reference spectrum (on the left) is produced by a mixture of tissues, including brain tissue. As the amount of brain tissue increases, the spectrum trends toward the spectrum produced by brain tissue alone (as shown on the right).

With this in mind, one can predict the behaviour of the final dispersion spectrum in response to changes in anatomy and tissue properties. For example, **Table 3** identifies the ivory table bone as having the lowest positive dispersive trend of the tissues presently included in the model. By decreasing the depth of the ivory table bone, the weight of its low dispersion is reduced. As a result, decreasing the depth promotes a high, positive overall dispersion. This results in a spectral expansion if the dispersion spectrum previously exhibited overall positive dispersion. On the other hand, decreasing the depth will cause the spectrum to contract if the overall dispersion spectrum previously exhibited overall negative dispersion.

Similarly, the behaviour of the final dispersion spectrum can be predicted for other changes. As a general guide, one must first deduce what type of dispersion (high, low, positive, negative) is being promoted by the change. Secondly, a contraction or expansion of the final spectrum will depend upon the relative properties of the other tissues contributing to the dispersion spectrum. Using these guidelines, logical causes for contraction and expansion are outlined in **Table 6**.

Causes of Spectral Contraction	Causes of Spectral Expansion
<ul style="list-style-type: none"> • Increase depth of tissue with relatively low or negative dispersion • Decrease depth of tissue with relatively high dispersion • Decrease in dispersion trend, any tissue 	<ul style="list-style-type: none"> • Increase depth of tissue with relatively high dispersion • Decrease depth of tissue with relatively low or negative dispersion • Increase in dispersion trend, any tissue

Table 6: Potential causes of spectral contraction and expansion. These guidelines apply to frequency sets with overall positive dispersion ($f > \tilde{f}$); corresponding guidelines for the opposite case ($f < \tilde{f}$) are obtained by interchanging ‘Increase’ \leftrightarrow ‘Decrease’.

For more detailed analysis, the IDM can be used to simulate the effects of certain changes. Varying model parameters within reasonable limits corresponds to real-life variations in the patient and test environment. The simulated dispersion patterns can then be used to exclude, and perhaps to determine, possible causes of the observations. In this spirit, the model has been used to simulate possible scenarios that might have produced the dispersion pattern observed in the second examination in **Figure 12**. This analysis is presented below.

Placement of transducers. During an examination with the DUS, the transducers are placed on the temples of the head, as described in Section 2.1. A possible explanation of the variation observed in **Figure 12** is that the transducer placement changed somewhat from one examination to the next. This scenario can be simulated in the IDM by varying the depths of the tissues; representative results are shown in **Figure 14**.

Notice that increasing the depth of the ivory table bones causes the overall dispersion spectrum to slightly contract. The contraction exhibited is, however, substantially less than that observed between the first and second examinations. As a result, a variation in depth of the ivory table bones alone could not have caused the observed variation between the first and second examinations.

Independently *increasing* the depth of the brain tissue or *decreasing* the depth of the diploë causes the dispersion spectrum to significantly contract. Independently or in combination, these two variations could contract the spectrum enough for it to

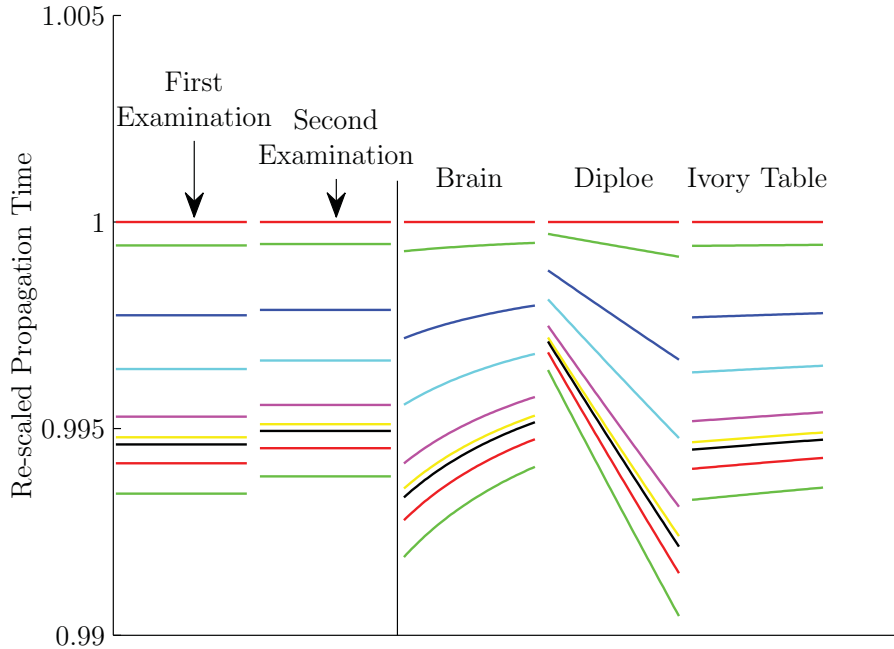


Figure 14: Dispersion spectra under various conditions related to transducer placement. The two spectra on the left are the same as those shown in **Figure 12**. On the right are three spectra showing how the "First Examination" spectrum might vary as the ultrasound transducer is moved. The examples labelled "Diploe" and "Ivory Table" were generated by varying the depth of the specified tissue over the ranges given in **Table 2**; for the "Brain" example the depth was varied over the range 80 to 130 mm.

resemble the spectrum produced by the second examination. As a result, increasing the depth of the brain and/or decreasing the depth of the diploë could have caused the observed variation. (Assuming that only one of the tissues was affected, the depth of brain tissue would have to increase from 110 mm to 122 mm, or the depth of diploë would have to decrease from 3.7 mm to 3.3 mm.)

Intracranial tissue anatomy. A change in the anatomy of the patient's intracranial tissues could also potentially have caused the observed variation between the two dispersion spectra in **Figure 12**. The change in anatomy could be pathological. For instance, given the attenuation and dispersion data available, we can simulate the dispersion pattern of hematomas of varying severity. Greater depths of blood correspond to more severe hematomas; see **Figure 15** for results.

Increasing the depth of blood causes the dispersion spectrum to contract. Hence, in principle the contraction observed in the second examination could have been caused by a hematoma within the patient's head. A layer of blood roughly 25 mm in depth

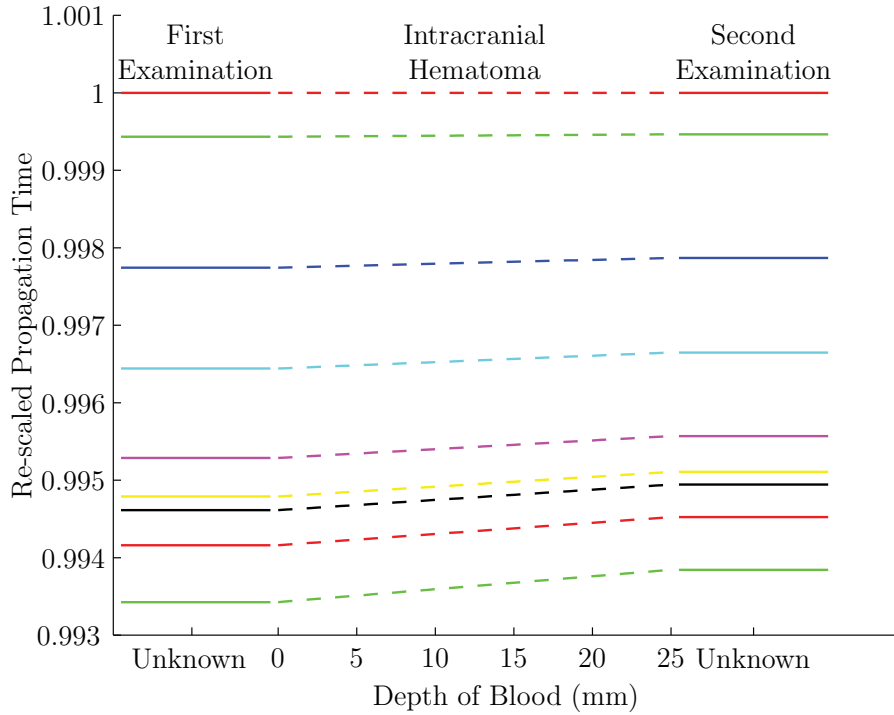


Figure 15: Dispersion spectra under the influence of an intracranial hematoma. The left and right spectra are as shown in **Figure 12**; the middle spectrum shows how an intracranial hematoma can cause the first spectrum to drift toward the second.

would be necessary to achieve the amount of contraction observed in the second examination.

Environmental factors. Other factors, such as the temperature and density of the tissues, affect the base propagation speed of the ultrasonic wave in a frequency dependent manner and therefore cause changes to the dispersion spectrum. The IDM can model these effects as well. **Figure 16** shows the spectral changes induced by varying the base propagation speed of the various tissues by $\pm 10\%$.

Varying the base speed within the ivory tables of the skull has only a small impact on the overall dispersion. As a result, such variations could not have caused the difference observed between the first and second examinations.

Decreasing the base speed within the brain tissue causes the overall dispersion spectrum to contract, and so could in principle be a cause of the observed data. However, as shown, the spectral contraction is significantly less than that observed.

Increasing the base speed within the diploë causes the overall dispersion spectrum to contract. Furthermore, the dispersion spectrum with diploë at maximal base

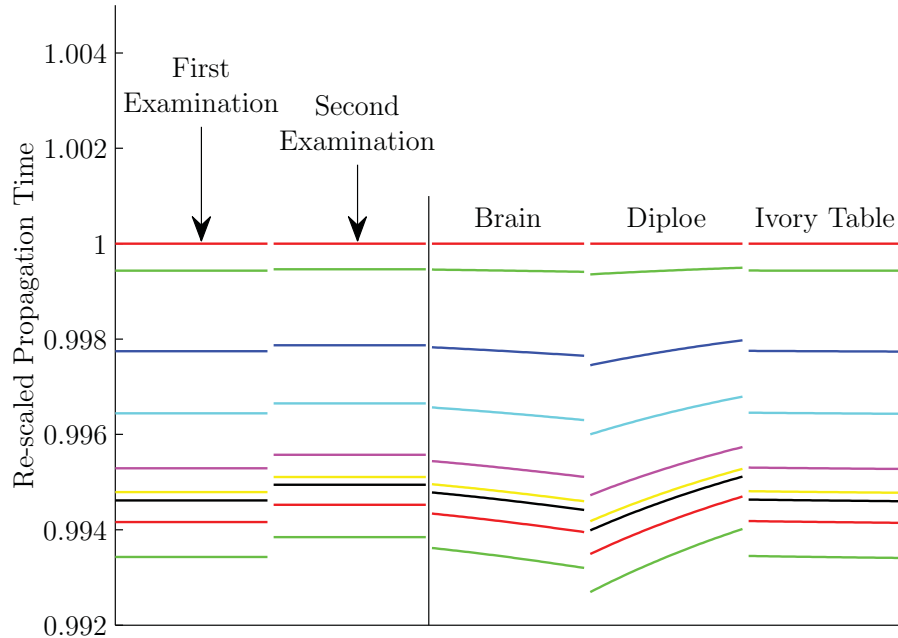


Figure 16: Dispersion spectra under various conditions related to changes in base propagation speed. The two spectra on the left are the same as those shown in **Figure 12**. On the right are three spectra showing how the "First Examination" spectrum might vary as factors affecting base propagation speed, such as temperature and pressure, are varied. The examples were generated by varying the base speed of the specified tissue by $\pm 10\%$ around the central values given in **Table 4**.

speed (see **Table 4**) converges to the spectrum observed in the second examination. As a result, a base speed variation, perhaps resulting from pressure or temperature changes within the diploë, could have caused the variation between the first and second examination.

3.2.1 Case study conclusions

In the preceding Section, we have considered a number of possible causes for the spectral contraction observed in **Figure 12**. Through simulation, certain possible causes were eliminated. For example, an increase in the depth of the ivory table skull bone as a result of inconsistent transducer placement, though it would produce a spectral contraction, was eliminated as a sole cause because it would not be able to produce a contraction as large as that observed. Of course, it could still be a contributing factor in combination with another cause.

Table 7 shows a set of possible causes of the spectral contraction that could not be eliminated in this way. These possible causes produce a contraction that is proportional to that observed in **Figure 12**. Discrimination between these possible causes would be made on the basis of the fine detail of the inter-line spacing in the dispersion spectrum; in the DUS, this discrimination task is the responsibility of a machine-learning classifier. We discuss the implications of the IDM for a machine-learning system in more detail in Section **3.3**.

In this case study, it was not possible to identify a single specific cause of the observed spectral contraction using the IDM alone. Although one of the potential causes was identified as being pathological (an intracranial hematoma), others were benign. This is likely to be true in general, especially considering that multiple factors may contribute to a single observed spectral change. Therefore, the IDM is not to be considered a substitute for a machine-learning approach to diagnosis, but rather as a complimentary approach that can be used, for example, to validate the conclusions reached by a machine-learning classifier, or to simulate the effects of certain pathologies.

Possible Cause of the Observed Spectral Contraction	Relevant Tissue	Quantity Change
Transducer placement	Brain	Increased depth
Transducer placement	Diploë	Decreased depth
Pathology	Blood	Increased depth
Pressure / Temperature variation	Diploë	Increased base speed

Table 7: Possible causes of the spectral contraction shown in **Figure 12**. In each case the quantity change is understood as being limited by the ranges given in **Tables 2 to 4**.

3.3 Implications for machine-learning systems

In practice, the DUS is designed to be used together with a machine-learning system to arrive at a diagnosis of intracranial injury. The analysis presented in this document has several implications for the performance of such a diagnostic system.

A machine-learning system, such as a Support Vector Machine or neural network, functions as a classifier: it assigns a dispersion spectrum collected from a subject to one of several classes, each class corresponding to a particular diagnosis. The machine-learning classifier is trained in advance to recognize the general features of each class. The principal advantages of a machine-learning approach to classification are, first, that the classification is fairly tolerant of minor variations between cases, which is useful in real-world applications where data are sometimes messy, and, second, that

the classification is automatically based on whatever features of the dispersion spectra provide the best discrimination between classes, without the user needing to specify in advance what those features are.

A re-scaled dispersion spectrum responds to a change in the insonified tissues in a way that depends on the collective properties of the tissues. There will always be a frequency, denoted \tilde{f} , which has the longest propagation time and which is therefore used to normalize the propagation times of the other frequencies; the frequency set is usefully divided into two subsets consisting respectively of frequencies above or below the reference frequency \tilde{f} . We found in Section **2.4.2** that the spectral lines for each subset are ordered by frequency and that, except in rare special cases, the spectral lines for each subset either expand or contract together; furthermore the two subsets generally respond in a manner opposite the other – when one expands the other contracts, and vice versa. Also, although the times for the two subsets are ordered by frequency, the times for the two frequency sets are, in general, intermixed, so that the entire set of times is not ordered by frequency.

Clearly, when the reference frequency \tilde{f} is the lowest (highest) frequency, as happens when positive (negative) dispersion media sufficiently dominate the spectrum, then all of the spectral lines expand or contract together. This uniformity implies that there are relatively fewer features by which a machine-learning classifier can distinguish one spectrum from another, and this may have an impact on the classification accuracy.

We speculate, on the basis of these considerations, that a machine-learning classifier will succeed well in some cases and less well in others. Specifically, we expect that, all other things (signal quality, number of frequencies, appropriateness of training data, etc.) being equal, the classifier will have a good chance of success when the insonified tissues are a mixture of positive and negative dispersion media, since in these cases spectral lines in a normalized spectrum will have a distinctive ordering. Conversely, when the set of tissues is dominated by either positive or negative dispersion media the spectral lines will be simply ordered by frequency and the machine-learning system will have to classify based principally on features such as inter-spectral line spacing. It is quite possible, however, that these finer details, being less distinctive, will provide less discriminatory power to the classifier, and thus less diagnostic accuracy.

According to **Table 3**, the principal tissues along the intracranial propagation path are positive dispersion tissues. This fact leads one to expect that the dispersion spectrum should have the relatively simple form in which the entire set of spectral lines are ordered by frequency. Experience, however, is a great teacher, and there is no substitute for real laboratory data. As was discussed in Section **2.3**, recent measurements of cancellous bone suggest that the diploë skull tissue, which is cancellous, may behave as a negative dispersion medium; if true, this would potentially complicate the observed spectrum in ways favourable to machine classification.

We hope that these speculations will stimulate further work on the machine-learning system for the DUS, and that experiments will investigate whether or not our expectations are realized in practice.

4 Conclusions

We have developed a model of ultrasonic dispersion in intracranial tissues that is intended to provide insight into the operation of DRDC's DUS and contribute to the success of DRDC's ongoing research program in diagnostic applications of dispersive ultrasound. The principal objective of the dispersive ultrasound research program is to develop safe, portable, and easy to use diagnostic tools to aid in the rapid diagnosis of non-visible neurological injury, with special attention to injuries resulting from blast exposure.

The DUS, which currently exists in the prototype stage, uses ultrasonic signals of different frequencies to characterize and monitor the state of internal tissues, and relies on a trained machine-learning classifier to produce a diagnosis. The IDM developed in this report is intended to complement that approach by giving greater insight into the dispersive effects of relevant tissues and pathologies.

We have carried out a literature review of the acoustic propagation characteristics, including the dispersive properties, of intracranial bone and tissue. We find that data are available for tissues comprising roughly 90% of the ultrasound signal's intracranial propagation path. The fact that some data are unavailable prevents the IDM being used to predict observed dispersion spectra at the present time.

In this report, we make a linear dispersion approximation, although the IDM could be readily generalized to include non-linear dispersion if data of sufficiently high quality were to become available. We review the relationship between acoustic dispersion and attenuation, and we derive the dispersion relation for human blood from its attenuation curve. We also discuss possible sources of negative dispersion and consider the implications of negative dispersion tissues for the interpretation of observed dispersion spectra, including the probable impact on a machine-learning classifier.

We also study, both analytically and numerically, how dispersion spectra respond to specific changes in the properties of tissues along the acoustic propagation path. We note certain special conditions under which changes to the tissues can nonetheless result in no change to the observed dispersion spectrum. We propose a convenient quantitative measure of the variation produced in a dispersion spectrum as a result of some change to the insonified tissues, and we use this measure to identify the factors to which intracranial dispersion spectra are most sensitive.

Finally, we examine the impact of the DUS's time resolution limits on both frequency

selection and diagnostic sensitivity, and we present a hypothetical case study to illustrate the diagnostic insights that can be gained from use of the IDM. We close with a discussion of the implications for machine-learning classifiers such as that used by the DUS.

We believe that these analyses demonstrate the value of the IDM, and we hope that it will contribute to the further success of DRDC's dispersive ultrasound research program.

References

- [1] Stergiopoulos, S., Freibert, A., Zhang, J., and Hatzinakos, D. (2008), Non-invasive monitoring of vital signs and traumatic brain injuries, (DRDC TR 2008-105) Defence R&D Canada – Toronto.
- [2] Wei, M., Stergiopoulos, S., Freibert, A., and Zhang, J. (2010), Dispersive ultrasound technology for quality control applications. DRDC Toronto Internal Publication.
- [3] Talairach, J. and Tournoux, P. (1988), Co-Planar Stereotaxic Atlas of the Human Brain, Thieme Medical Publishers.
- [4] Lynnerup, N., Astrup, J., and Sejrsen, B. (2005), Thickness of the human cranial diploe in relation to age, sex and general body build, *Head & Face Medicine*, 1, 13.
- [5] Pakula, M., Padilla, F., and Laugier, P. (2009), Influence of the filling fluid on frequency-dependent velocity and attenuation in cancellous bones between 0.5 and 2.5 MHz, *Journal of the Acoustical Society of America*, 126(6), 3301–3310.
- [6] BrainLink, The Brain - Understanding the Nervous System (online), <http://www.brainlink.org.au/understanding-the-nervous-system.htm> (Access Date: 17 March 2011).
- [7] Droin, P., Berger, G., and Laugier, P. (1998), Velocity dispersion of acoustic waves in cancellous bone, *IEEE Transactions on Ultrasonics, Ferroelectrics, and Frequency Control*, 45(3), 581–592.
- [8] Wear, K. (2000), Measurements of phase velocity and group velocity in human calcaneus, *Ultrasound in Medicine and Biology*, 26(4), 641–646.
- [9] Wear, K. (2007), Group velocity, phase velocity, and dispersion in human calcaneus in vivo, *Journal of the Acoustical Society of America*, 121(4), 2431–2437.
- [10] Kremkau, F., Barnes, R., and McGraw, C. (1981), Ultrasonic attenuation and propagation speed in normal human brain, *Journal of the Acoustical Society of America*, 70(1), 29–38.
- [11] Fry, F. and Barger, J. (1978), Acoustical properties of the human skull, *Journal of the Acoustical Society of America*, 63(5), 1576–1590.
- [12] Yoon, H. and Katz, J. (1979), Temperature dependence of the ultrasonic velocities in bone, In *Proceedings of the 1979 Ultrasonics Symposium*, IEEE Ultrasonics, Ferroelectrics, and Frequency Control Society.

- [13] Hill, C., Bamber, J., and ter Haar, G., (Eds.) (2002), *Physical Principles of Medical Ultrasonics*, Second ed, Wiley.
- [14] Duck, F. (1990), *Physical Properties of Tissue: A Comprehensive Reference Book*, Academic Press.
- [15] Crossman, A. and Neary, D. (2010), *Neuroanatomy: An Illustrated Colour Text*, Fourth ed, Churchill Livingstone. p.57.
- [16] Rengachary, S. and Ellenbogen, R., (Eds.) (2005), *Principles of Neurosurgery*, Elsevier Mosby.
- [17] He, P. (1999), Experimental verification of models for determining dispersion from attenuation, *IEEE Transactions on Ultrasonics, Ferroelectrics, and Frequency Control*, 46(3), 706–714.
- [18] Szabo, T. (2004), *Diagnostic Ultrasound Imaging: Inside Out*, Elsevier Academic Press. p.75.
- [19] Arfken, G. (1985), *Mathematical Methods for Physicists*, Third ed, Academic Press. p.426.
- [20] O'Donnell, M., Jaynes, E., and Miller, J. (1981), Kramers-Kronig relationship between ultrasonic attenuation and phase velocity, *Journal of the Acoustical Society of America*, 69, 696–701.
- [21] Lee, C., Lahham, M., and Martin, B. (1990), Experimental verification of the Kramers-Kronig relationship for acoustic waves, *IEEE Transactions on Ultrasonics, Ferroelectrics, and Frequency Control*, 37, 286–294.
- [22] Szabo, T. (1994), Time domain wave equations for lossy media obeying a frequency power law, *Journal of the Acoustical Society of America*, 96, 491–500.
- [23] Szabo, T. (1995), Causal theories and data for acoustic attenuation obeying a frequency power law, *Journal of the Acoustical Society of America*, 97, 14–21.
- [24] Waters, K., Hughes, M., Mobley, J., Brandenburger, G., and Miller, J. (2000), On the applicability of Kramers-Kronig relations for ultrasonic attenuation obeying a frequency power law, *Journal of the Acoustical Society of America*, 108, 556–563.
- [25] Gurumurthy, K. and Arthur, R. (1982), A dispersive model for the propagation of ultrasound in soft tissues, *Ultrasonic Imaging*, 4, 355–377.
- [26] Kuc, R. (1984), Modeling acoustic attenuation of soft tissue with a minimum-phase filter, *Ultrasonic Imaging*, 6, 24–36.

- [27] Waters, K. and Hoffmeister, B. (2005), Kramers-Kronig analysis of attenuation and dispersion in trabecular bone, *Journal of the Acoustical Society of America*, 118(6), 3912–3920.
- [28] Anderson, C., Bauer, A., Marutyan, K., Holland, M., Pakula, M., Bretthorst, G., Laugier, P., and Miller, J. (2011), Bone Quantitative Ultrasound, Ch. Phase velocity of cancellous bone: Negative dispersion arising from fast and slow waves, interference, diffraction, and phase cancellation at piezoelectric receiving elements, pp. 319–330, Springer.
- [29] Plona, T., Winkler, K., and Schoenberg, M. (1987), Acoustic waves in alternating fluid/solid layers, *Journal of the Acoustical Society of America*, 81(5), 1227–1234.
- [30] Wear, K. (2001), A stratified model to predict dispersion in trabecular bone, *IEEE Transactions in Ultrasonics, Ferroelectrics, and Frequency Control*, 48(4), 1079–1083.
- [31] Marutyan, K., Holland, M., and Miller, J. (2006), Anomalous negative dispersion in bone can result from the interference of fast and slow waves, *Journal of the Acoustical Society of America*, 120(5 Pt 1), EL55–61.
- [32] Anderson, C., Marutyan, K., Holland, M., Wear, K., and Miller, J. (2008), Interference between wave modes may contribute to the apparent negative dispersion observed in cancellous bone, *Journal of the Acoustical Society of America*, 124(3), 1781–1789.
- [33] Bauer, A., Marutyan, K., Holland, M., and Miller, J. (2008), Negative dispersion in bone: the role of interference in measurements of the apparent phase velocity of two temporally overlapping signals, *Journal of the Acoustical Society of America*, 123(4), 2407–2414.

Acronyms

CSF	Cerebrospinal Fluid
DRDC	Defence Research and Development Canada
DUS	Dispersive Ultrasound System
IDM	Intracranial Dispersion Model
mTBI	mild Traumatic Brain Injury
TBI	Traumatic Brain Injury

Distribution list

DRDC Toronto TM 2011-042

Internal distribution

- 5 Author
- 1 Library

Total internal copies: 6

External distribution

- 1 Casualty Management Section
Defence R&D Canada – Suffield
Box 4000, Stn Main
Medicine Hat, Alberta
T1A 8K6
Attn: Stephen Bjarnason
Stephen.Bjarnason@drdc-rddc.gc.ca
- 1 Andreas Freibert
296 Hendon Avenue
Toronto, ON
M2M 1B2
Andreas.Freibert@gmail.com

Total external copies: 2

Total copies: 8

This page intentionally left blank.

DOCUMENT CONTROL DATA		
(Security classification of title, body of abstract and indexing annotation must be entered when document is classified)		
<p>1. ORIGINATOR (The name and address of the organization preparing the document. Organizations for whom the document was prepared, e.g. Centre sponsoring a contractor's report, or tasking agency, are entered in section 8.)</p> <p>Defence R&D Canada – Toronto 1133 Sheppard Avenue West, PO Box 2100, Toronto ON M3M 3B9, Canada</p>	<p>2. SECURITY CLASSIFICATION (Overall security classification of the document including special warning terms if applicable.)</p> <p>UNCLASSIFIED (NON-CONTROLLED GOODS) DMC A, Review: GCEC June 2010</p>	
<p>3. TITLE (The complete document title as indicated on the title page. Its classification should be indicated by the appropriate abbreviation (S, C or U) in parentheses after the title.)</p> <p>Intracranial Dispersion Model</p>		
<p>4. AUTHORS (Last name, followed by initials – ranks, titles, etc. not to be used.)</p> <p>Burrell, C.; Chauhan, P.</p>		
<p>5. DATE OF PUBLICATION (Month and year of publication of document.)</p> <p>January 2012</p>	<p>6a. NO. OF PAGES (Total containing information. Include Annexes, Appendices, etc.)</p> <p>56</p>	<p>6b. NO. OF REFS (Total cited in document.)</p> <p>33</p>
<p>7. DESCRIPTIVE NOTES (The category of the document, e.g. technical report, technical note or memorandum. If appropriate, enter the type of report, e.g. interim, progress, summary, annual or final. Give the inclusive dates when a specific reporting period is covered.)</p> <p>Technical Memorandum</p>		
<p>8. SPONSORING ACTIVITY (The name of the department project office or laboratory sponsoring the research and development – include address.)</p> <p>Defence R&D Canada – Toronto 1133 Sheppard Avenue West, PO Box 2100, Toronto ON M3M 3B9, Canada</p>		
<p>9a. PROJECT OR GRANT NO. (If appropriate, the applicable research and development project or grant number under which the document was written. Please specify whether project or grant.)</p> <p>14ei05</p>	<p>9b. CONTRACT NO. (If appropriate, the applicable number under which the document was written.)</p>	
<p>10a. ORIGINATOR'S DOCUMENT NUMBER (The official document number by which the document is identified by the originating activity. This number must be unique to this document.)</p> <p>DRDC Toronto TM 2011-042</p>	<p>10b. OTHER DOCUMENT NO(s). (Any other numbers which may be assigned this document either by the originator or by the sponsor.)</p>	
<p>11. DOCUMENT AVAILABILITY (Any limitations on further dissemination of the document, other than those imposed by security classification.)</p> <p><input checked="" type="checkbox"/> Unlimited distribution <input type="checkbox"/> Defence departments and defence contractors; further distribution only as approved <input type="checkbox"/> Defence departments and Canadian defence contractors; further distribution only as approved <input type="checkbox"/> Government departments and agencies; further distribution only as approved <input type="checkbox"/> Defence departments; further distribution only as approved <input type="checkbox"/> Other (please specify):</p>		
<p>12. DOCUMENT ANNOUNCEMENT (Any limitation to the bibliographic announcement of this document. This will normally correspond to the Document Availability (11). However, where further distribution (beyond the audience specified in (11)) is possible, a wider announcement audience may be selected.)</p> <p>UNLIMITED</p>		

13. ABSTRACT (A brief and factual summary of the document. It may also appear elsewhere in the body of the document itself. It is highly desirable that the abstract of classified documents be unclassified. Each paragraph of the abstract shall begin with an indication of the security classification of the information in the paragraph (unless the document itself is unclassified) represented as (S), (C), or (U). It is not necessary to include here abstracts in both official languages unless the text is bilingual.)

We present a model of ultrasonic dispersion in intracranial tissues that is intended to provide insight into the operation of DRDC Toronto's Dispersive Ultrasound System and contribute to the success of DRDC's ongoing research program in diagnostic applications of dispersive ultrasound. The Dispersive Ultrasound System is designed to use the dispersion spectrum produced by acoustic signals as they traverse the skull and intracranial tissue to identify non-visible neurological injuries, such as those resulting from blast exposure.

The Intracranial Dispersion Model is a mathematical representation of intracranial tissues and their acoustic dispersive properties. It has been developed in order to better understand the formation of dispersion spectra and the effects that various factors, including intracranial injury, have upon them. The formulation of the Intracranial Dispersion Model is presented in detail. We study, both analytically and numerically, how dispersion spectra respond to specific changes in the properties of tissues along the ultrasound propagation path. We also examine uncertainties in dispersion measurements and their diagnostic implications. Finally, a hypothetical case study illustrates the diagnostic insights that can be gained from use of the Intracranial Dispersion Model.

14. KEYWORDS, DESCRIPTORS or IDENTIFIERS (Technically meaningful terms or short phrases that characterize a document and could be helpful in cataloguing the document. They should be selected so that no security classification is required. Identifiers, such as equipment model designation, trade name, military project code name, geographic location may also be included. If possible keywords should be selected from a published thesaurus. e.g. Thesaurus of Engineering and Scientific Terms (TEST) and that thesaurus identified. If it is not possible to select indexing terms which are Unclassified, the classification of each should be indicated as with the title.)

Ultrasonics; Ultrasound; Acoustic Dispersion; Medical Diagnostics; Neurological Injury; Blast Exposure; Tissue Characterization

Defence R&D Canada

Canada's Leader in Defence
and National Security
Science and Technology

R & D pour la défense Canada

Chef de file au Canada en matière
de science et de technologie pour
la défense et la sécurité nationale



www.drdc-rddc.gc.ca

